AEDC-TR-80-51

C.2

An Investigation of the Techniques of Ellipsometry, Internal Reflection Spectroscopy, and Moment Analysis to the Study of Films and Substrates

Kent F. Palmer, Department of Physics, and
Michael Z. Williams, Department of Mathematics
Westminster College, Fulton, Missouri

January 1981

Final Report for Period October 1, 1979 – September 1, 1980

ARNOLD ENGINEERING DEVELOPMENT CENTER
ARNOLD AIR FORCE STATION, TENNESSEE
AIR FORCE SYSTEMS COMMAND
UNITED STATES AIR FORCE

NOTICES

When U. S. Government drawings, specifications, or other data are used for any purpose other than a definitely related Government procurement operation, the Government thereby incurs no responsibility nor any obligation whatsoever, and the fact that the Government may have formulated, furnished, or in any way supplied the said drawings, specifications, or other data, is not to be regarded by implication or otherwise, or in any manner licensing the holder or any other person or corporation, or conveying any rights or permission to manufacture, use, or sell any patented invention that may in any way be related thereto.

Qualified users may obtain copies of this report from the Defense Technical Information Center.

References to named commercial products in this report are not to be considered in any sense as an indorsement of the product by the United States Air Force or the Government.

This report has been reviewed by the Office of Public Affairs (PA) and is releasable to the National Technical Information Service (NTIS). At NTIS, it will be available to the general public, including foreign nations.

APPROVAL STATEMENT

This report has been reviewed and approved.

KENNETH H. LENERS
Project Manager
Directorate of Technology

Approved for publication:

FOR THE COMMANDER

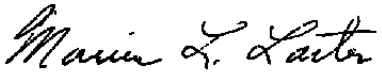

MARION L. LASTER
Director of Technology
Deputy for Operations

REPORT DOCUMENTATION PAGE		READ INSTRUCTIONS BEFORE COMPLETING FORM
1. REPORT NUMBER AEDC-TR-80-51	2 GOVT ACCESSION NO.	3. RECIPIENT'S CATALOG NUMBER
4. TITLE (and Subtitle) AN INVESTIGATION OF THE TECHNIQUES OF ELLIPSOMETRY, INTERNAL REFLECTION SPECTROSCOPY, AND MOMENT ANALYSIS TO THE STUDY OF FILMS AND SUBSTRATES		5 TYPE OF REPORT & PERIOD COVERED Final Report-October 1, 1979 to September 1, 1980 6 PERFORMING ORG. REPORT NUMBER
7. AUTHOR(s) Kent F. Palmer and Michael Z. Williams, Westminster College, Fulton, Missouri 65251		8 CONTRACT OR GRANT NUMBER(s)
9 PERFORMING ORGANIZATION NAME AND ADDRESS Arnold Engineering Development Center/DOT Air Force Systems Command Arnold Air Force Station, Tennessee 37389		10. PROGRAM ELEMENT, PROJECT, TASK AREA & WORK UNIT NUMBERS Program Element 65807F
11 CONTROLLING OFFICE NAME AND ADDRESS Arnold Engineering Development Center/DOS Air Force Systems Command Arnold Air Force Station, Tennessee 37389		12 REPORT DATE January 1981 13 NUMBER OF PAGES 69
14 MONITORING AGENCY NAME & ADDRESS(if different from Controlling Office)		15 SECURITY CLASS. (of this report) UNCLASSIFIED 15a DECLASSIFICATION/DOWNGRADING SCHEDULE N/A

16 DISTRIBUTION STATEMENT (of this Report)

Approved for public release; distribution unlimited.

17 DISTRIBUTION STATEMENT (of the abstract entered in Block 20, if different from Report)

18 SUPPLEMENTARY NOTES

Available in Defense Technical Information Center (DTIC)

19 KEY WORDS (Continue on reverse side if necessary and identify by block number)

ellipsometers	substrates	cryogenics
internal reflection	infrared spectra	
spectroscopy	visible spectra	
measurements	analysis	
films	moments	

20 ABSTRACT (Continue on reverse side if necessary and identify by block number)

Ellipsometry and internal reflection spectroscopy (IRS) are two methods of spectroscopic measurement which have some unique advantages over other reflection techniques for the study of films and substrates. Applications of these methods are fully discussed for work in the infrared and visible spectral regions. Moment analysis of spectral band shapes has been shown theoretically to yield information on the nature of the intermolecular interactions

DD FORM 1 JAN 73 1473 EDITION OF 1 NOV 65 IS OBSOLETE

20. ABSTRACT (Continued)

in condensed phases. These data are vital if concentrations of molecular species are to be found in a film. The experimental difficulties of moment analysis are discussed along with some preliminary results using existing AEDC data. Areas for future research are suggested for the spectroscopic analysis of films.

AFSC
Arnold AFS Tenn

PREFACE

The research reported herein was performed by Westminster College, Fulton, Missouri, under Subcontract No. 80-25-PWT for ARO, Inc. (a Sverdrup Corporation Company), operating contractor of Arnold Engineering Development Center, Air Force Systems Command, Arnold Air Force Station, Tennessee. The work covered the period from October 1, 1979, to September 1, 1980, and was done under ARO Project Number P32K-13C. Dr. Herman E. Scott, Directorate of Technology, was the Air Force project manager. The manuscript was submitted for publication on September 19, 1980.

CONTENTS

ILLUSTRATIONS

TABLE

1.0 INTRODUCTION

Spectroscopic techniques have been used extensively for the identification of molecular species and the determination of molecular structure. For gases and condensed phases whose absorption laws are known, molecular species concentrations can be found. The accuracies of molecular identification and species concentration depend on the precision of the spectroscopic methods. In this report two reflection sepctroscopic methods prove, in some instances, to be superior to more conventional reflection or transmission techniques.

At the turn of the century, Paul Drude developed a method for the analysis of polarized light reflected from surfaces. The method, now called ellipsometry, is especially sensitive to thin-film formation on a substrate, but it is primarily used for the near infrared (IR), visible, and near ultraviolet (UV) spectral regions where suitable optics are readily available. On the other hand, internal reflection spectroscopy (IRS) can be readily applied throughout the IR spectral region. IRS spectra are very sensitive to the optical constants, and even weak absorptions can be observed by using multiple reflections. Ellipsometry and IRS methods are explored in Sections 2.0 and 3.0.

In condensed phases of molecules, intermolecular effects become much more important than they are for the gas phase, and condensed phase spectra have broader and more blended absorption features than do the gas phase spectra of the same species. Consideration of the molecular interactions is important if molecular species concentrations are to be found in solid or liquid films (Refs. 1 and 2). Because moment analyses of spectral band shape can be interpreted in terms of intermolecular interactions, we have thoroughly investigated the band shapes of existing AEDC cryofilm data and presented the results in Section 4.0. Areas for future research are suggested in Section 5.0.

2.0 ELLIPSOMETRY

A light beam reflected from an interface of two media is altered in its state of polarization from the incident beam. The change in polarization is affected by the optical constants and the geometry of the media. If, in addition, other nearby interfaces can cause multiple reflection effects (e.g., the two interfaces of a thin lamellate film sandwiched between a semi-infinite ambient medium and a semi-infinite substrate), then the optical constants and geometry of all interacting media affect the change in polarization. Analyses of the changes in polarization by the techniques of ellipsometry are especially useful for determining the optical properties of a substrate material having a large extinction coefficient, k, or finding the optical constants and thickness of a very thin, uniform film on a substrate. The use of small-diameter light beams allows the extraction of spatial

information about surfaces. Howéver, the standard optical materials used in currently available commercial ellipsometers limit the spectral domain to the visible, near-IR, and near-UV. With optional quartz optics, measurements may be made from 2.5 micrometers to 0.21 μm. Ellipsometric methods in the IR will be discussed later.

An article by Neal (Ref. 3) contains an excellent overview of ellipsometry and an extensive bibliography. A more advanced and thorough treatment of ellipsometric methods is given by Assam and Bashara (Ref. 4).

2.1 REFLECTION OF A MONOCHROMATIC ELLIPTICALLY POLARIZED LIGHT BEAM

A classical monochromatic beam has a wavetrain that is infinite in extent and completely polarized (Ref. 5). The time- and space-variant electric field associated with the light beam can be represented as the resultant of two mutually perpendicular vectors having a constant phase difference between them.

Let the electric field disturbance $\vec{E}$ of a beam propagating in the z direction of a right-handed coordinate system be represented by the real part of $\hat{E}(z, t)\vec{u}$, where the circumflex denotes a complex quantity, t is time, and $\vec{u}$ is a unit vector in the x-y plane. In Fig. 1 (adapted from Ref. 6) x is oriented parallel to the plane of incidence. $\hat{E}(z, t)\vec{u}$ can be decomposed into the sum of the p component

$$\hat{E}_p(z, t) = E_{po} \exp\left\{-i\left[\omega(t - \hat{n}_o z/c) + a_p\right]\right\} \tag{1}$$

which is parallel to the plane of incidence in the direction of unit vector $\vec{u}_p$ and the s component

$$\hat{E}_s(z, t) = E_{so} \exp\left\{-i\left[\omega(t - \hat{n}_o z/c) + a_s\right]\right\} \tag{2}$$

which is perpendicular to the plane of incidence in the direction of the unit vector $\vec{u}_s$. Thus,

$$\hat{E}(z, t)\vec{u} = \hat{E}_s(z, t)\vec{u}_s + \hat{E}_p(z, t)\vec{u}_p$$

$$= \sum_\ell E_{\ell o} \exp\left\{-i\left[\omega(t - n_o z/c) + a_\ell\right]\right\} \vec{u}_\ell, \ \ell = p, s \tag{3}$$

Here, $\omega = 2\pi c\nu$ is the angular frequency of the wave, c is the speed of light in vacuo, and ν is the vacuum wavenumber, which is the reciprocal of the vacuum wavelength, λ. Note that in Muller's convention for ellipsometric notation (Ref. 7), the time dependence of the

electromagnetic field is exp(+iωt) so that the complex index of refraction of a medium is $\hat{n} = n - iK$. In spectroscopy, the time dependence is usually as exp(—iωt) so that $\hat{n} = n + iK$.

In Fig. 1, the constant phase difference $\alpha \equiv \alpha_p - \alpha_s$ is indicated as well as the relative positions of the maxima of each component. In all practical cases the incident medium is nonabsorbing (i.e., $\hat{n}_o = n_o$). The wavetrain is plane-polarized if α is an integer multiple of π, and elliptically polarized otherwise.

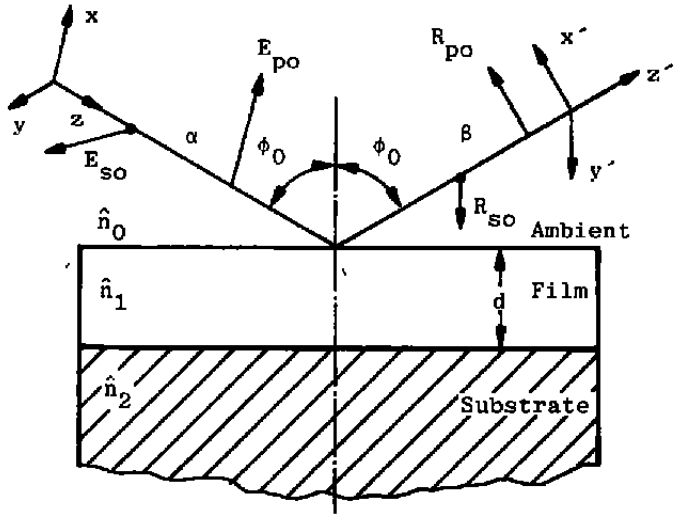

Figure 1. Reflection of an elliptically polarized light wave.

From Fig. 1 and Eqs. (1) through (3), we may write

$$E_p(z, t) = \mathrm{Re}\left\{\hat{E}_p(z, t)\right\} = E_{po}\cos(\theta + \alpha) \tag{4}$$

and

$$E_s(z, t) = \mathrm{Re}\left\{\hat{E}_s(z, t)\right\} = E_{so}\cos\theta \tag{5}$$

for the p and s components of the electric field, where

$$\theta = \omega(t - n_o z/c) + \alpha_s \tag{6}$$

is a function of t and z. From Eq. (4) we have

$$E_p/E_{po} - \cos\theta\cos\alpha = -\sin\theta\sin\alpha$$

which upon squaring yields

$$\left(E_p^2/E_{po}^2\right) - 2\,(E_p/E_{po})\cos\theta\cos\alpha + \cos^2\theta\cos^2\alpha = \sin^2\theta\sin^2\alpha$$

Substituting $\cos\theta = E_s/E_{so}$ from Eq. (5), then rearranging terms, gives

$$\frac{E_p^2}{E_{po}^2} + \frac{E_s^2}{E_{so}^2} - \frac{2\,E_p\,E_s\cos\alpha}{E_{po}\,E_{so}} = \sin^2\alpha \tag{7}$$

Equation (7) describes an ellipse, as can be shown by the descriminant test described in analytical geometry texts. The semimajor axis, a, and semiminor axis, b, are

$$a = \sin\alpha \Bigg/ \left(\frac{\cos^2\eta}{E_{po}^2} - \frac{\sin^2\eta}{E_{so}^2} + \frac{\sin 2\eta\cos\alpha}{E_{so}\,E_{po}}\right)^{1/2} \tag{8}$$

$$b = \sin\alpha \Bigg/ \left(\frac{\sin^2\eta}{E_{po}^2} + \frac{\cos^2\eta}{E_{so}^2} - \frac{\sin 2\eta\cos\alpha}{E_{so}\,E_{po}}\right)^{1/2} \tag{9}$$

These results may be ascertained by performing a rotation by η of the x- and y-axes about the z-axis of Fig. 1 with use of the transformation

$$\begin{pmatrix} E_p \\ E_s \end{pmatrix} = \begin{pmatrix} \cos\eta & -\sin\eta \\ \sin\eta & \cos\eta \end{pmatrix} \begin{pmatrix} E_x' \\ E_y' \end{pmatrix} \tag{10}$$

where E_x' and E_y' are the components of $\vec{E} = \mathrm{Re}(\hat{E})\vec{u}$ that are parallel to the semimajor and semiminor axes, respectively.

The value of the phase difference α between the p and s components determines not only the shape and orientation of the elliptical path traced by the electric field vector $\vec{E}$, as the above equations indicate, but also the sense of its rotation. If α is an integer multiple of π, Eq. (7) reduces to a constant proportionality between E_p and E_s, i.e.,

$$E_s = \pm \left(E_{po}/E_{so}\right) E_p$$

and the orientation of $\vec{E}$ is confined to a plane, i.e., $\vec{u}$ is constant. If α is within the first or second quadrants, $\vec{E}$ appears to rotate clockwise when looking into the beam. If α is within the third or fourth quadrants, the rotation is counterclockwise.

Upon reflection at the interface of two media, the electric field, $\vec{R}$, of the reflected beam can be represented by

$$\vec{R}(z', t) = \mathrm{Re}\left\{\hat{R}(z', t)\right\} \vec{u}' \tag{11}$$

where

$$\hat{R}(z', t)\,\vec{u}' = \hat{R}_p(z', t)\,\vec{u}'_p + \hat{R}_s(z', t)\,\vec{u}_s$$

$$= \Sigma R_{\ell_o} \exp\left\{-i\left[\omega\left(t - \hat{n}_o z'/c\right) - \beta_\ell\right]\right\} \vec{u}_\ell$$

$$\ell = p, s$$

Here, z' is the direction of propagation of the reflected wave, $\vec{u}'$ is in the x'-y' plane of the x'- y'- z' axes of Fig. 1, $\vec{u}'_p$ and $\vec{u}'_s$ (both perpendicular to z') are unit vectors along the p and s directions, respectively, the constant phase difference between the p and s components of $\vec{R}$ is $\beta \equiv \beta_p - \beta_s$, and

$$\hat{R}_\ell(z, t) = R_{\ell_o} \exp\left\{-i\left[\omega\left(t - \hat{n}_o z'/c\right) - \beta_\ell\right]\right\}$$

$$\ell = p, s \tag{12}$$

In general, $\vec{R}$ is also elliptically polarized: Again, note that n_o is usually real in ellipsometric experiments.

2.2 THE ELLIPSOMETRIC PARAMETERS ψ and Δ

An ellipsometer measures the change in the polarization states of the incident and the reflected (or, very rarely, the refracted) light beams. In essence, E_s is altered in the reflection process to become R_s, and E_p changes to R_p. The information about the change in polarization is contained in the complex ratio of ratios

$$\hat{\rho} \equiv \frac{\hat{R}_p/\hat{E}_p}{\hat{R}_s/\hat{E}_s} = \frac{\hat{R}_p/\hat{R}_s}{\hat{E}_p/\hat{E}_s} \tag{13}$$

evaluated at the boundary. Equations (1), (2), (12), and (13) give

$$\hat{\rho} = \frac{\left|R_{po}/R_{so}\right| \exp\left[i(\beta_s - \beta_p)\right]}{\left|E_{po}/E_{so}\right| \exp\left[i(\alpha_s - \alpha_p)\right]} \tag{14}$$

$$= \tan\psi \exp(-i\,\Delta)$$

where

$$\tan\psi = \frac{|R_{po}/R_{so}|}{|E_{po}/E_{so}|} \tag{15}$$

and

$$\Delta = \beta - \alpha \tag{16}$$

are the conventionally defined quantities for the ratio of the electric field amplitude ratios and the change in the phase difference, respectively.

2.3 ELIPSOMETER COMPONENTS

An ellipsometer is an instrument that can produce a collimated beam of elliptically polarized light which can be reflected from a sample system (S) and then checked for the changes of polarization caused by the reflection process. Many instrument geometries are possible, but all ellipsometers include (1) a collimated monochromatic light source, L; (2) a polarizer, P; (3) a sample system mount, which may be oriented vertically (for solid samples only) or horizontally (for solid and liquid samples); (4) an analyzer, A, itself a polarizer, and (5) a detector system, D. In addition, most ellipsometers contain (6) a compensator, C. Figure 2, adapted from Refs. 4 and 6, shows a typical ellipsometer geometry known as the PCSA configuration.

2.3.1 Light Sources

The collimated monochromatic light source may consist of a conventional polychromatic light source, a narrow band filter, slit, and collimating lens system. Lasers are also used. Commercial optics are available that allow a He-Ne (helium-neon) laser beam (0.6328 μm) to be reduced to a cross-sectional diameter of 25 μm or smaller. This allows spatial testing of thin films and surfaces.

2.3.2 Polarizers and Analyzers

The partially polarized or unpolarized radiation from a light source will be plane-polarized upon passing through a polarizer. Nicol, Glan, and Glan-Thompson prisms are often used as polarizers or analyzers from the near IR to the near UV. In the medium and far IR, the non-normal transmission of a beam through stacks of thin transparent plates can cause satisfactory plane-polarization. Other IR polarizers include the double Glan prism (Ref. 8). Plane-polarized light from the polarizer can be converted to elliptically-polarized light by a compensator. The orientation of a plane-polarized wave can be found with the

orientation of a polarizer used as an analyzer. The polarizer, analyzer, and compensator are mounted on rotators capable of accurate angular determination, e.g., ±0.01 deg.

2.3.3 Compensators or Retarders

The phase difference between two components of a wave can be altered upon passing through a compensator, which allows one component to pass through faster than the other. Mica and calcite are two examples of noncubic anisotopic crystalline materials which are birefringent, i.e., materials within which a normally incident beam of light is divided into two rays, (1) a ray nearly undeviated in its path (the "ordinary" ray) and (2) an "extraordinary" ray, which is noticeably deflected. A thin birefringent plate will allow a normally incident plane-polarized wave to exit a plane-polarized wave only when its plane of polarization cuts the plate surfaces in two mutually perpendicular directions in the plane of the plate surfaces.

The directions of the lines of intersection are the privileged directions; the speeds of propagation differ in the two privileged directions. In the plate, the "slow" component of an incident wave parallel to the slow direction follows the path of the ordinary ray with an effective index n_o, and the "fast" component follows the extraordinary path with an effective index $n_e < n_o$.

The phase shift δ, or the relative retardation, of the plate can be found by considering the fast component, $E_o(z, t)$, and the slow component, $E_e(z, t)$, of the electric vector, $\vec{E}(z, t)$, of a plane-polarized light beam normally incident upon a thin birefringent plate. If $z = o$ at the front surface, then the form of each component within the plate is, from Eqs. (1) and (2),

$$\mathrm{Re}\left\{E_{\ell_o} \exp\left\{-i\left[\omega\,(t - n_\ell\, z/c) - a_o\right]\right\}\right\} \quad ; \quad \ell = o, e$$

If the deflection of the two components is negligible for a thin birefringent plate of thickness τ, the final change in phase between components is

$$\delta = \frac{\omega\tau}{c}\,(n_o - n_e) = 2\pi\nu\tau(n_o - n_e) \tag{17}$$

If ellipsometric measurements are made at a single vacuum wavenumber, ν, the equations given below can be simplified if τ is chosen so that $\delta = \pi/2$. Such a plate is termed a quarter-wave compensator.

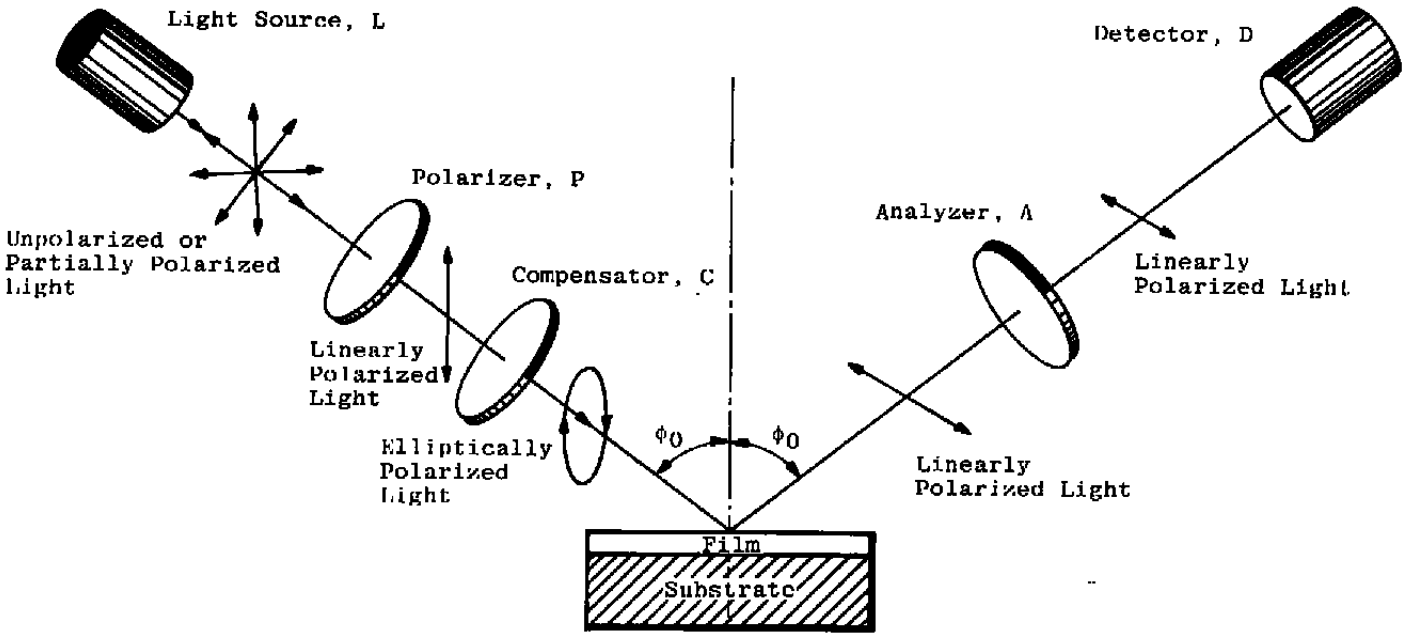

Figure 2. Typical ellipsometer arrangement: the polarizer-compensator-sample system-analyzer (PCSA) configuration.

Phase differences, δ, can be varied during an experiment by using a Babinet-Soleil compensator (Ref. 5), or a Pockels effect retarder (Ref. 9). The latter consists of a plate of ammonium dihydrogen phosphate (ADP), which becomes birefringent when a potential difference exists across its thickness.

2.3.4 Detector Systems

The detector system is usually an electro-optical device such as a photomultiplier tube (PMT) for near IR to near UV measurements, or, for IR work, a photovoltaic, photoconductor, or pyroelectric detector. For measurements over a wide spectral range, the detector system can be a spectrophotometer (Ref. 8). Often a telescope is used in conjunction with the electro-optical system to make the preliminary settings of the optical components. Fine adjustments are made either manually or automatically by a feedback signal monitoring the output of the detector system.

2.4 ELLIPSOMETRIC TECHNIQUES FOR THE MEASUREMENTS OF ψ AND Δ

The methods of ellipsometric measurements fall into five categories (Ref. 10). The first four discussed are null techniques in which ellipsometer components are rotated to allow a minimum of light to pass through an analyzer. Thus, the light incident upon the analyzer must be plane-polarized, or very nearly so.

If the compensator precedes the sample system in the optical train, as in the PCSA arrangement of Fig. 2, the orientations of the components must be such that the beam incident upon the sample is properly elliptically polarized so that the reflected beam is plane-polarized. (In the PSCA arrangement, the compensator follows the sample system, the beam incident upon the sample is plane-polarized.) The elliptically-polarized beam reflected from the sample becomes plane-polarized again after passing through the properly oriented compensator. The four general methods of null ellipsometry differ in regard to which components are adjusted to achieve the null condition, namely the extinction of the beam by the analyzer.

2.4.1 The Variable Retardation Null Method

The variable retardation method permits a direct measurement of the phase difference, Δ. At a fixed orientation of the fast axis, the phase shift, δ, of a variable compensator (e.g., a Babinet-Soleil compensator or a Pockels effect retarder) is adjusted as well as the orientation of either the polarizer or analyzer. At null, the phase difference of the beam and

the phase shift of the compensator are equal (i.e., $\Delta = \delta$), and the orientation of the rotating polarizer, or analyzer, gives ψ.

This method is not as accurate as other methods if manual adjustments of δ are made. However, the use of an electro-optical retarder gives a measuring precision comparable to that of other null methods.

2.4.2 The Quarter-Wavelength Compensator Null Method

In the quarter-wavelength compensator method, either the polarizer (in the PSCA configuration) or the analyzer (in a PCSA arrangement) has its axis set at $\pm(\pi/4)$ relative to the plane of incidence. The unfixed component and compensator are rotated until the null condition appears. Some care must be exercised because the settings of the two components are not independently adjustable.

Deriving the appropriate relations for computing the ψ and Δ parameters from the experimental settings involves much algebra (Ref. 11). If in a PSCA arrangement, the polarizer axis setting is $\pm(\pi/4)$ from the plane of incidence, if the angle of the fast axis of the compensator relative to the plane of incidence is X, and if the angle between the fast axis and analyzer is γ, then $E_{po}/E_{so} = 1$, $\tan\psi = R_{po}/R_{so}$, $\alpha = 0$, and $\beta = \Delta$

Let the equation of the ellipse traced out by the electric vector, $\vec{R}$, of the reflected beam be

$$\frac{R_x''^2}{c^2} + \frac{R_y''^2}{d^2} = 1 \tag{18}$$

where the components R_x'' and R_y'' are referred to a coordinate axis frame x''y''z'' formed after rotation by x about the z'- axis of the x'- y'- z' reference frame of Fig. 1. These components are related to the p and s components of $\vec{R}$, R_p, and R_s, respectively, by the transformation inverse to 10:

$$\begin{pmatrix} R_x'' \\ R_y'' \end{pmatrix} = \begin{pmatrix} \cos x & \sin x \\ -\sin x & \cos x \end{pmatrix} \begin{pmatrix} R_p \\ R_s \end{pmatrix} \tag{19}$$

The analysis of this elliptically polarized reflected beam is entirely analogous to that of the elliptically polarized beam given in Section 2.1. Thus, the elliptical axes c and d can be chosen to be

$$c = \sin\beta \Bigg/ \left(\frac{\cos^2 x}{R_{po}^2} + \frac{\sin^2 x}{R_{so}^2} + \frac{\sin 2x \cos\beta}{R_{po} R_{so}} \right)^{1/2} \tag{20}$$

and

$$d = \sin\beta \Bigg/ \left(\frac{\sin^2 x}{R_{po}^2} + \frac{\cos^2 x}{R_{so}^2} - \frac{\sin 2x \cos\beta}{R_{po} R_{so}} \right)^{1/2} \tag{21}$$

and the relation for the angle of rotation, x, from the plane of incidence is

$$\tan 2x = \frac{2 R_{po} R_{so} \cos\beta}{R_{so}^2 - R_{po}^2} \tag{22}$$

If Eqs. (20) and (21) are squared, then added, we have

$$\sin^2\beta \left(\frac{c^2 + d^2}{c^2 d^2} \right) = \frac{R_{so}^2 + R_{po}^2}{R_{so}^2 R_{po}^2} \tag{23}$$

Transformation of Eq. (19) produces

$$c^2 + d^2 = R_{so}^2 + R_{po}^2 \tag{24}$$

The ellipticity, γ, of the ellipse traced out by the head of $\vec{R}$ is defined in the relation

$$\tan\gamma \equiv d/c = \frac{\sin\gamma}{\cos\gamma} \tag{25}$$

Thus, choosing $c = A\cos\gamma$ gives $d = A\sin\gamma$. Of course, $R_{po} = R_o \sin\psi$, and $R_{so} = R_o \cos\psi$ in the present case, and from Eq. (24), $A = R_o$. Substituting Eqs. (24) and (25) into Eq. (23) yields

$$\sin^2\beta \cos^2\psi \sin^2\psi = \cos^2\gamma \sin^2\gamma$$

or

$$\sin^2 2\gamma = \sin^2 2\psi \sin^2\beta$$

or

$$\sin 2\gamma = \pm \sin 2\psi \sin\Delta \tag{26}$$

where the substitution $\Delta = \beta$ is made. Also, from Eq. (22),

$$\tan 2x = \frac{2\left(R_{po}/R_{so}\right)\cos\beta}{1 - R_{po}^2/R_{so}^2} = \left(\frac{2\tan\psi}{1-\tan^2\psi}\right)\cos\Delta$$

or

$$\tan 2x = \tan 2\psi \cos\Delta \tag{27}$$

We next find the relations for Δ and ψ reciprocal to Eqs. (26) and (27). Squaring Eq. (26) and noting $\sin^2\theta = 1 - \cos^2\theta$ produces

$$\cos^2 2\gamma = \cos^2 2\psi\left[1 - \cos^2\Delta\left(\frac{1}{\cos^2 2\psi} - 1\right)\right]$$

or

$$\cos 2\gamma = \cos 2\psi\,(1 + \cos^2\Delta \tan^2 2\psi)^{1/2}$$

which, upon substitution of Eq. (27), is

$$\cos 2\gamma = \cos 2\psi\,(1 + \tan^2 2\gamma)^{1/2} = \cos 2\psi/\cos 2x$$

or

$$\cos 2\psi = \cos 2\gamma \cos 2x \tag{28}$$

Eq. (27) may also be written as

$$(\sin 2x)/(\cos 2x) = \left[(\sin 2\psi)/(\cos 2\psi)\quad \cos\Delta\right]$$

Substituting $\sin 2\psi = \pm[(\sin 2\gamma)/(\sin\Delta)]$ from Eq. (26) and for $\cos 2\psi$ from Eq. (28) gives

$$\sin 2x = \pm\left[\frac{(\sin 2\gamma)/(\sin\Delta)}{\cos 2\gamma}\right]\cos\Delta$$

or

$$\tan\Delta = \pm\left(\frac{\tan 2\gamma}{\sin 2x}\right) \tag{29}$$

Corrections for slight deviations from the ideal quarter-wave compensator phase shift of $\pi/2$ have been given by Plumb (Ref. 12). We should note, however that the quarter-wave null method must be done at discrete wavelengths, which are determined by the availability of suitable compensators. The next null method overcomes this limitation.

2.4.3 The Fixed Compensator Null Method

In the fixed compensator method of ellipsometry, the fast axis is set at a fixed angle to the plane of incidence — usually $\pm(\pi/4)$ — and the null occurs by adjusting the polarizer and the analyzer. Either the PCSA (Fig. 2) or the PSCA configurations may be used. The rather lengthy derivation of the ellipsometric relations for ψ and Δ in the fixed compensator method will now be shown.

For a PCSA ellipsometer arrangement, consider the plane-polarized beam transmitted by the polarizer with an electric vector $\vec{E}_i = E_i\vec{u}_i$ (Fig. 3) where $\vec{u}_i$ is a unit vector in the plane of the electric field and perpendicular to the propagation direction. The magnitude, E_i, of the electric field is the real part of

$$\hat{E}_i = E_{io} \cdot \exp\left\{-i\left[\omega(t - n_o z/c) - \alpha_i\right]\right\} \tag{30}$$

In Fig. 3, the angle P (measured by the polarizer) is the angle of the plane of the electric field with the plane of incidence. The beam is incident upon the compensator, whose fast axis makes an angle, C, with the plane of incidence.

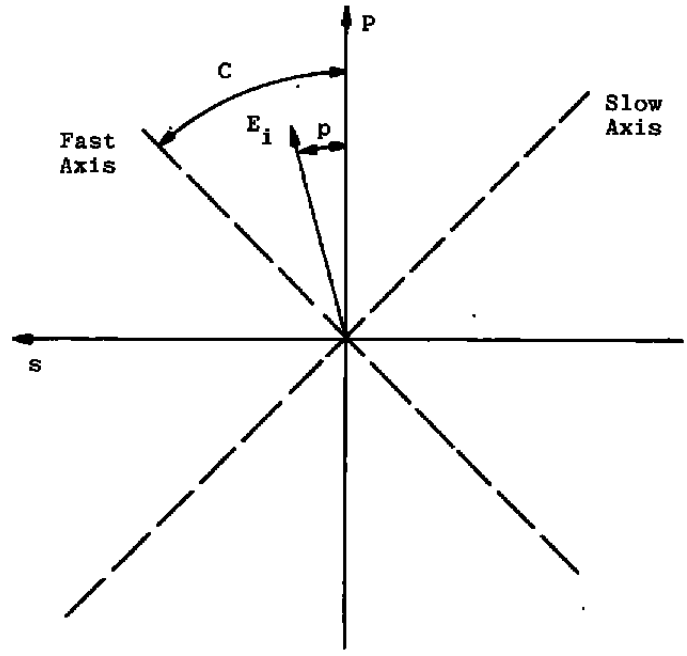

Figure 3. Electric field of a beam emerging from the polarizer.

The fast and slow components, $\hat{E}_e$ and $\hat{E}_o$, respectively, of the complex amplitude, $\hat{E}_i$, are

$$\hat{E}_e = \hat{E}_i \cdot \cos (C - P) \tag{31}$$

and

$$\hat{E}_o = -\hat{E}_i \cdot \sin (C - P) \tag{32}$$

The corresponding amplitude components, $\hat{E}_e'$ and $\hat{E}_o'$, of the elliptically polarized beam transmitted by the compensator are

$$\hat{E}_e' = f_e \cdot \hat{E}_i \cdot \cos (C - P) \cdot e^{i\delta} \tag{33}$$

and

$$\hat{E}_o' = -f_o \cdot \hat{E}_i \cdot \sin (C - P) \tag{34}$$

The phase lead, δ, of the fast component is attributable to the compensator; f_e and f_o respectively represent the fractions of the incident amplitudes of the fast and slow components that exit the compensator. The relationships among (1) the p and s components of the complex amplitude of the elliptically polarized beam exiting the compensator and (2) the fast and slow components of the electric field are given by the transformation in Eq. (10):

$$\begin{pmatrix} \hat{E}_p \\ \hat{E}_s \end{pmatrix} = \begin{pmatrix} \cos C & -\sin C \\ \sin C & \cos C \end{pmatrix} \begin{pmatrix} \hat{E}_e' \\ \hat{E}_o' \end{pmatrix}$$

$$= \hat{E}_i \begin{pmatrix} f_e \cos (C - P) \cos C\, e^{i\delta} + f_o \sin (C - P) \sin C \\ f_e \cos (C - P) \sin C\, e^{i\delta} - f_o \sin (C - P) \cos C \end{pmatrix} \tag{35}$$

It is often assumed that $f_e = f_o$; i.e., the compensator is perfectly dichroic, and the differences in multiple reflection effects along the two optical axes are negligible. Deviations from ideal behavior have been observed (Ref. 13), and corrections for real compensators will be discussed after the $f_e = f_o$ case is considered.

Let us assume that $f_e = f_o$ and choose $C = \pm(\pi/4)$ so that $\sin C = \cos C$. From Eq. (35),

$$\frac{\hat{E}_p}{\hat{E}_s} = \frac{1 + \cot (\pi/4 - P) e^{i\delta}}{-1 + \cot (\pi/4 - P) e^{i\delta}} \tag{36}$$

Following Archer and Shank (Ref. 14), we will show that, for the ratio tan L of the magnitude of the p and s amplitudes, i.e.,

$$\tan L = \left| \hat{E}_p / \hat{E}_s \right| \tag{37}$$

and for the phase difference Δ' between the p and s components, Eq. (36) yields

$$\tan \Delta' = \tan (2P - \pi/2) \cdot \sin \delta \tag{38}$$

and

$$\cos 2L = -\cos 2P \cos \delta \tag{39}$$

If the numerator and denominator of Eq. (36) are both multiplied by the complex conjugate of the denominator and if the appropriate trigonometric identities are inserted, we obtain

$$\frac{\hat{E}_p}{\hat{E}_s} = \frac{\cot^2 \theta - 1 - 2i \cot \theta \sin \delta}{\csc^2 \theta - 2 \cot \theta \cos \delta}$$

$$= \frac{\left[(\cot^2 \theta - 1)^2 + 4 \cot^2 \theta \sin^2 \delta\right]^{1/2}}{\csc^2 \theta - 2 \cot \theta \cos \delta} \exp\left[i \tan^{-1} \left(\frac{-2 \cot \theta}{\cot^2 \theta - 1} \sin \delta \right) \right]$$

$$= \tan L \exp (i\Delta') \tag{40}$$

where

$$\theta = (\pi/2) - P \tag{41}$$

From the identities

$$\tan 2x = (\cot 2x)^{-1} = (2 \cot x)/(\cot^2 x - 1)$$

and

$$\tan \Delta' = -\tan 2\theta \sin \delta = \tan (-2\theta) \sin \delta \tag{42}$$

the above equation becomes Eq. (38) upon substitution of Eq. (41).

The moduli of Eq. (40) are also equal; therefore,

$$\tan^2 L = \frac{\cot^2 2\theta + \sin^2 \delta}{(\csc 2\theta - \cos \delta)^2} \tag{43}$$

if a factor of $4 \cot^2 \theta$ is extracted from both the numerator and denominator of the squared modulus and if

$$\sin 2x = 2 \sin x \cos x \tag{44}$$

is invoked along with the identity in Eq. (42). Noting that

$$\tan^2 L = \frac{1 - \cos 2L}{1 + \cos 2L} \tag{45}$$

and solving for cos 2L in terms of θ and δ, we obtain upon simplification

$$\cos 2L = \frac{\csc^2 2\theta - 2\csc 2\theta \cos \delta - \cos^2 \delta - \cot^2 2\theta - \sin^2 \delta}{\csc^2 2\theta - 2\csc 2\theta \cos \delta + \cos^2 \delta - \cot^2 2\theta + \sin^2 \delta} \tag{46}$$

When the identities

$$1 = \sin^2 x + \cos^2 x = \csc^2 x - \cot^2 x \tag{47}$$

are inserted into Eq. (46), we find

$$\cos 2L = \frac{\cos \delta (\cos \delta - \csc 2\theta)}{\csc \theta (\csc 2\theta - \cos \delta)} = -\sin 2\theta \cos \delta \tag{48}$$

Equation (48) becomes identical to Eq. (39) when

$$\sin 2\theta = \cos 2P \tag{49}$$

is used.

Now the relations must be found for the parameters ψ and Δ in the fixed compensator mode of null ellipsometry. Because the reflected beam is plane-polarized, and, thus, the phase differences β, between the p and s components of the electric field of the reflected beam are integer multiples of π, the change in the phase difference, Δ, is either

$$\Delta_1 = -\Delta', \quad \text{for } \beta = 2\ell\pi \tag{50}$$

or

$$\Delta_2 = -\Delta' + \pi, \quad \text{for } \beta = (2\ell - 1)\pi \tag{51}$$

where ℓ is an integer. These two values of Δ correspond to $\theta = (\pi/4 - P)$ ranges of $0 \leq \theta \leq \pi$ and $-\pi \leq \theta \leq 0$, respectively, so there are two extinction settings of the polarizer angle, e.g., P_1 and P_2. Because two distinct angles having the same tangent function value must differ by an odd multiple of π, we have from Eq. (39),

$$P_2 - P_1 = \pi/2 \tag{52}$$

A relation for ψ is obtained from the measurement of A, the angle of the analyzer from the plane of incidence at extinction. It is seen in Fig. 4 that the plane-polarized electric vector, $\vec{R}$, of the reflected beam is at the angle $A - (\pi/2)$, giving (from Fig. 4a)

$$\left| \frac{\hat{R}_p}{\hat{R}_s} \right| = -\cot (A_1 - \pi/2) = \tan (-A_1) \tag{53}$$

for $\pi/2 \leq A_1 \leq \pi$, and (from Fig. 4b)

$$\left| \frac{\hat{R}_p}{\hat{R}_s} \right| = \cot (A_2 - \pi/2) = \tan A_2 \tag{54}$$

from the definition of ψ, Eq. (15), and Eqs. (37), (53), and (54),

$$\tan \psi = \tan (-A_1) \cot L_1 = \tan A_2 \cot L_2 \tag{55}$$

for the two sets of extinction settings.

ψ can be related to measurable parameters from a consideration of the orientation of the electric vector. In Fig. 5, the electric vector incident upon the compensator is pictured for the two cases $P = P_1$ and $P = P_2 = P_1 + (\pi/2)$. We can see that the fast component of the electric vector for the case $P = P_1$ has an amplitude identical to the amplitude of the slow component in the case $P = P_2$, and vice versa. Thus, Eqs. (53) and (54) indicate

$$\tan L_2 = \cot L_1 \tag{56}$$

and, from, Eq. (55),

$$\tan^2 \psi = \tan (-A_1) \tan A_2 \tag{57}$$

It is important to note that in Eqs. (33) through (48) the compensator phase shift, δ, need not be $\pi/2$. This means that during an ellipsometric run, the wavenumber of the radiation may be varied without replacing the fixed phase shift compensator. This represents a distinct advantage over the quarter-wavelength compensator null method.

If C were chosen to be $-(\pi/4)$, the steps outlined above would produce relationships among the ellipsometric parameters ψ and Δ and the instrumental settings P and A, which are similar to Eqs. (50), (51), and (57).

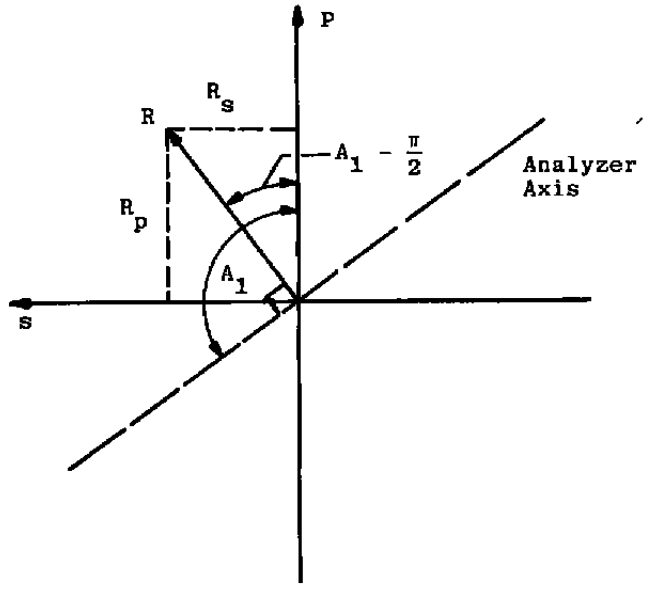

a. Analyzer angle $> \pi/2$

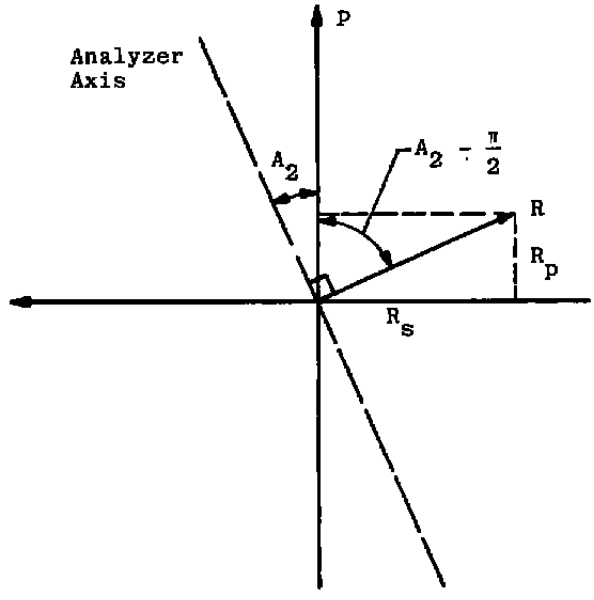

b. Analyzer angle $< \pi/2$

Figure 4. Electric field of the plane-polarized beam incident upon the analyzer.

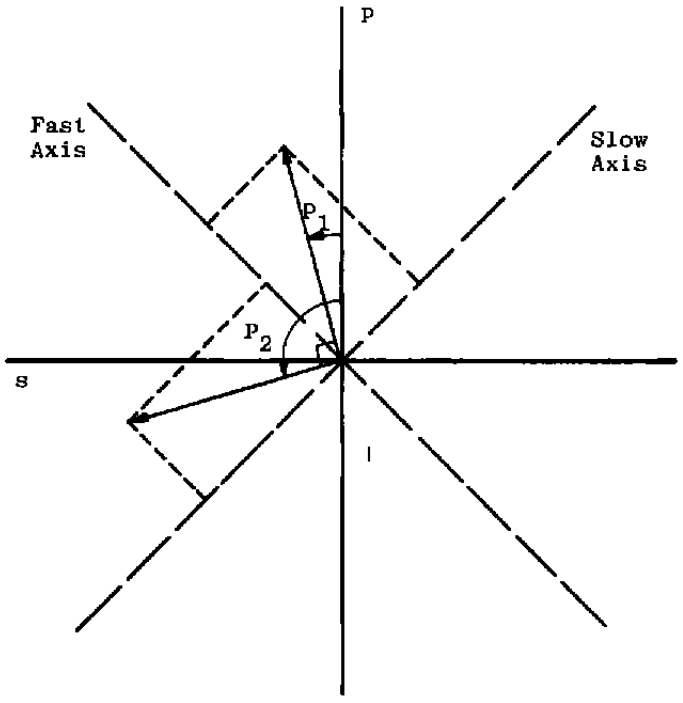

Figure 5. Relationship of the two possible polarizer angle values P_1 and P_2.

Archer and Shank (Ref. 14) have demonstrated empirically that many compensator plates have unequal beam attentuations along the fast and slow orientations; i.e., $f_e \neq f_o$. It may be that the multiple reflection effects within the plate are noticeably different along the two optical axes because of the differences in the refractive index, and/or the plates are pleochroic. This causes $P_2 - P_1 \neq \pi/2$, and it invalidates Eq. (38) for Δ'. However, Eq. (57) for ψ is still correct. Archer and Shank (Ref. 14) give the corrections necessary to compute Δ from the two measured null positions of the polarizer angle, P.

2.4.4 Principal Angle Null Methods

The principal angle of incidence, θ, is defined as the angle of incidence, ϕ_o, at which the change of phase difference, Δ, between the p and s components is, upon reflection, equal to $\pm(\pi/2)$. It has been found that the nulling schemes discussed above are usually most sensitive when the angle of incidence is near the principal angle. For a great many sample systems, θ is about 70 deg.

In most of the principal angle of incidence methods, the angle of incidence is varied until the principal angle of incidence is found for different fixed settings of the polarizer, compensator, and analyzer angles (Refs. 4, 15, 16, and 17). Kinosita and Yamamoto

describe one principal angle of incidence scheme in which the compensator is eliminated (Ref. 17). The primary advantage of these methods lies in the ease with which the optical parameters could be determined for $\Delta = \pm(\pi/2)$. However, these methods require more precise measurements of the angle of incidence to achieve the accuracy of other ellipsometric methods.

2.4.5 Nonextinction Methods

Most nulling schemes in ellipsometry require adjustments of at least two highly interdependent instrumental components. Precision measurements often take considerable time, even with the use of automatic ellipsometers. Rapid changes in surface conditions, such as those occurring during film formation, cannot be monitored. Special problems may sometimes be posed by the difficulty of obtaining precision compensators and polarizers for IR ellipsometry. Increased measuring speed and more accurate IR measurements are often obtained through observing intensity changes in the ellipsometer.

In most non-nulling ellipsometric techniques, all instrumental components except one are held at predetermined settings. The movable component, usually the analyzer, is rotated at a constant rate, and the output of the detector is electronically monitored for changes in intensity and phase. While changes in the ellipsometric parameters ψ and Δ can be closely followed, the accuracy of measurement of the optical parameters for this method is usually less than the accuracy attainable by nulling techniques. This is because of the imprecision associated with measurements of the varying intensity and phase. (See Refs. 4, 8, and 18 through 21.)

In many instances of nonextinction ellipsometry, both the compensator and its drawbacks can be eliminated. Such ellipsometric methods are particularly attractive for IR work (Refs. 8, 20, and 21) in which accurate intensity measurements are difficult to obtain. Stobie el at (Ref. 20) discuss an IR ellipsometer that, in some cases, does not require such critical, absolute intensity measurements. Their ellipsometer has a stationary polarizer and analyzer and a rotating polarizer (P_{rot}) in either P P_{rot} S A or a P S P_{rot} A configuration. By relating the component frequencies of the intensity variation to the phase shifts of the p and s components of the beam, one may calculate ψ and Δ.

In all ellipsometric intensity measurements, the quadrant in which a calculated angle lies cannot be determined because only the absolute values of amplitudes are observed. This means that good approximate values of the optical constants must be known prior to measurement so that the proper signs of angles can be inferred.

2.5 ERRORS ASSOCIATED WITH ELLIPSOMETER COMPONENTS

The errors in angular measurement and orientation and the spurious effects caused by reflections and depolarizations of the beam can be ascribed to all ellipsometer components. Some of the problems associated with imperfect compensators are discussed in Section 2.4.3. The causes and proposed corrections for many instrumental errors have been compiled and explored by Azzam and Bashara (Ref. 4). Error analysis depends to a large extent on the particular ellipsometric technique used and the ellipsometer configuration.

For many ellipsometric measurements, including those on cryogenic or ultraclean surfaces, an environmental chamber surrounding the sample system is required. The chamber windows become new optical components in the optical train of the ellipsometer and can be birefringent under the stress of a pressure differential of one atmosphere. Also, nonplanar and/or nonparallel window surfaces can cause deviations of the beam path.

Experimentally, the following procedure may be used for vacuum measurements of ψ and Δ (Ref. 3). After a vacuum measurement, the chamber is allowed to return to the ambient room pressure and temperature. During this time a clean surface will oxidize and a cryogenic film will evaporate. After the oxidation or evaporation is complete, the chamber may be pumped out again, and measurements of ψ and Δ repeated for the new surace in vacuo. After the chamber interior is once again at ambient pressure and temperature and the windows are removed, ψ and Δ are remeasured for the new surface. After the results are compared for the new surface at the two experimental conditions, the vacuum measurements of the original sample system can be corrected.

2.6 RELATIONSHIP OF THE ELLIPSOMETRIC PARAMETERS ψ AND Δ TO THE OPTICAL PROPERTIES OF THE SAMPLE SYSTEM

The optical properties of the system as well as its geometry directly affect the outcome of ellipsometric measurements of ψ and Δ (that is, if the optical properties and the geometry of a sample are known), the values of ψ and Δ can be computed. The inverse problem of extracting the sample optical properties and geometry from the ellipsometric measurements of ψ and Δ is the more common situation, and we shall consider their problem for the two sample cases of (1) a semi-infinite ambient and substrate, and (2) a uniform thin film sandwiched between a semi-infinite ambient and a semi-infinite substrate. In what follows we shall assume that all materials in the sample system are isotropic. (Anisotropic media are treated in Refs. 4 and 22.)

Figure 6 shows the planar interface of two semi-infinite media and a beam incident upon the interface at an angle ϕ_o. Adapting the notation of Ref. 1 to the case of non-normal incidence for two media n_i and n_j, we may write the complex Fresnel boundary conditions for the reflection coefficient, r_{ij}, and the transmission coefficient, t_{ij}, as (Ref. 23)

$$\hat{r}_{ijp} = \frac{\hat{n}_i \cos \phi_j - \hat{n}_j \cos \phi_i}{\hat{n}_i \cos \phi_j + \hat{n}_j \cos \phi_i} \tag{58}$$

$$\hat{t}_{ijp} = \frac{2\hat{n}_i \cos \phi_i}{\hat{n}_i \cos \phi_j + \hat{n}_j \cos \phi_i} \tag{59}$$

$$\hat{r}_{ijs} = \frac{\hat{n}_i \cos \phi_i - \hat{n}_j \cos \phi_j}{\hat{n}_i \cos \phi_i + \hat{n}_j \cos \phi_j} \tag{60}$$

and

$$\hat{t}_{ijs} = \frac{2\hat{n}_i \cos \phi_i}{\hat{n}_i \cos \phi_i + \hat{n}_j \cos \phi_j} \tag{61}$$

It is clear from Eqs. (58) through (61) that the p and s components do not behave in the same manner except at normal incidence.

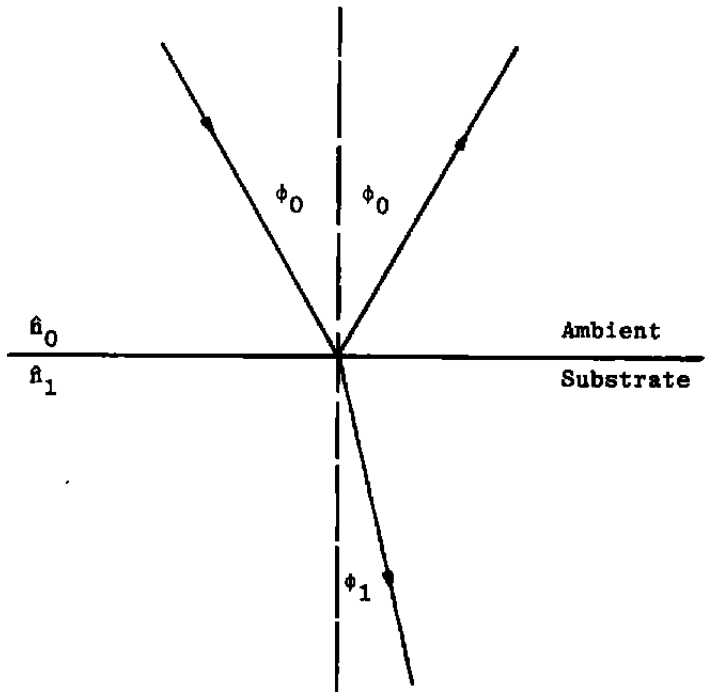

Figure 6. Reflection and refraction for an ambient-substrate system.

2.6.1 The Ambient-Substrate System

From the Fresnel relations [Eqs. (58) through (61)], Ditchburn (Ref. 24) has derived equations for the optical indices n_o and $\hat{n}_1$ for the case of a semi-infinite nonabsorbing ambient, i.e., $\hat{n}_o = n_o + ik_o = n_o$. These are (Refs. 25 and 26)

$$n_1^2 = n_o^2 \sin^2 \phi_o \left[1 + \frac{\tan^2 \phi_o \cos^2 2\bar{\psi}}{(1 + \sin 2\bar{\psi} \cos \bar{\Delta})^2} \right] \tag{62}$$

and

$$k_1 = \frac{n_o \tan \phi_o \sin \phi_o \sin 2\bar{\psi} \sin \bar{\Delta}}{1 + \sin 2\bar{\psi} \cos \bar{\Delta}} \tag{63}$$

$\bar{\psi}$ and $\bar{\Delta}$ represent the ellipsometric parameters of a film-free substrate; thus, the optical constants can be found for an ultraclean substrate.

Light beams in an absorbing medium such as a metal are not homogeneous (Ref. 5), so the optical constants change with the angle of incidence. Vasicek (Ref. 26) shows that the optical constants at normal incidence $\bar{\hat{n}} = \bar{n} + i\bar{k}$, are preferred, which he gives as

$$\bar{n}_1^2 = \frac{C + A}{2} \tag{64}$$

$$\bar{k}_1^2 = \frac{C - A}{2} \tag{65}$$

where

$$A = n_1^2 - k_1^2 = \bar{n}_1^2 - \bar{k}_1^2$$

$$B = 2n_1 k_1 \cos \phi_1 = 2\bar{n}_1 \bar{k}_1$$

$$C^2 = A^2 + B^2$$

and

$$\phi_1 = \cos^{-1} \sqrt{1 - \frac{n_0^2}{n_1^2} \sin^2 \phi_o} \tag{66}$$

2.6.2 The Ambient-Thin Film-Substrate System

In Fig. 7 it is assumed that the thin film is uniform and homogeneous and has parallel boundaries between the ambient and substrate media. Also, the substrate and the ambient are considered semi-infinite in extent: i.e., multiple reflection effects within the substrate and the ambient are assumed not to exist. For highly absorbing substrates (e.g., metals) which are actually thick films, this assumption seems justified because the virtual extinction of a beam in the substrate occurs over pathlengths on the order of a wavelength throughout most of the IR, visible, and near-UV spectral regions. For substrates which are dielectric thick films, however, multiple reflections at the dielectric interfaces can occur, and their effects have been successfully treated in conventional reflection (Ref. 27) and transmission (Ref. 21) spectroscopy. Nevertheless, we have yet to find in the literature a treatment of multiple reflection effects in a substrate applied to ellipsometric techniques, and feel that this topic may be an area of future interest.

The fundamental relations for the interpretation of ellipsometric measurements of an isotropic and lamellate thin film on a substrate were derived by Paul Drude in 1889. The complex reflection coefficient, r_{012}, for the thin film and substrate in Fig. 7 is (Refs. 2 and 25)

$$\hat{r}_{012\ell} = \left[\hat{r}_{01\ell} + \hat{r}_{12\ell} \exp(2i\hat{\gamma}_1 d)\right] \Big/ \left[1 + \hat{r}_{01\ell}\,\hat{r}_{12\ell} \exp(2i\hat{\gamma}_1 d)\right] \tag{67}$$

$$\ell = p, s$$

where

$$\hat{\gamma}_1 \equiv 2\pi\nu\hat{n}_1 \cos\phi_1 \tag{68}$$

and ϕ_1 can be found from Eq. (66) if the ambient is nonabsorbing. From Eqs. (13), (14), and (67), we may write

$$\tan\psi\, e^{-i\Delta} = \frac{\hat{r}_{01p} + \hat{r}_{12p} \exp(2i\hat{\gamma}_1 d)}{1 + \hat{r}_{01p}\,\hat{r}_{12p} \exp(2i\hat{\gamma}_1 d)} \cdot \frac{1 + \hat{r}_{01s}\,\hat{r}_{12s} \exp(2i\hat{\gamma}_1 d)}{\hat{r}_{01s} + \hat{r}_{12s} \exp(2i\hat{\gamma}_1 d)} \tag{69}$$

which is often called the "exact" Drude equation. Thus, ψ and Δ are complicated functions of nine parameters: ν, ϕ_o, and d, and the real and imaginary parts of $\hat{n}_o$, $\hat{n}_1$, and $\hat{n}_2$.

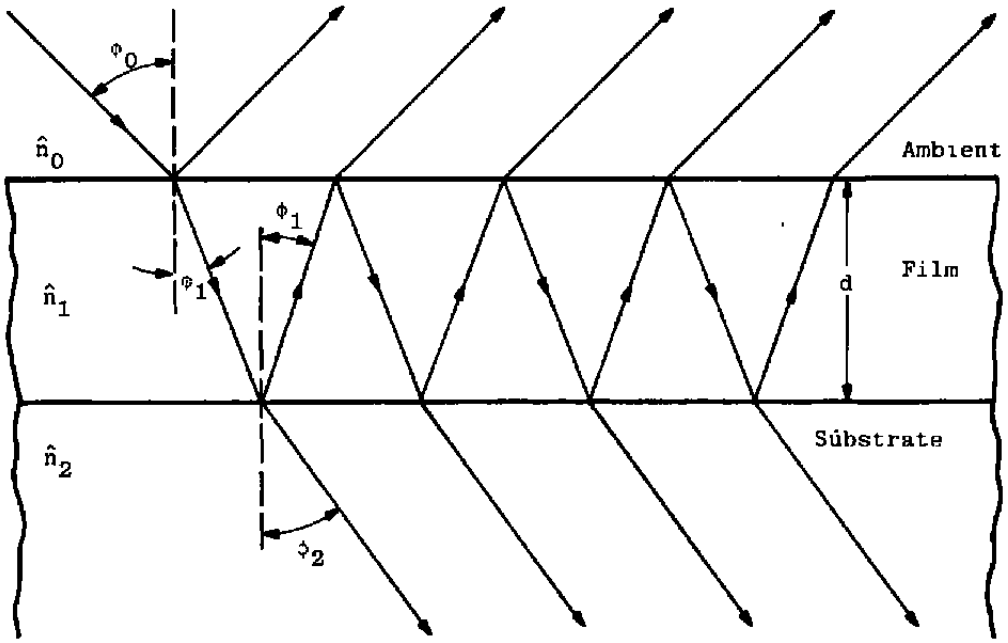

Figure 7. Reflection and refraction for an ambient-thin film-substrate system.

The inversion of the real and imaginary parts of Eq. (69) to solve for any of the nine parameters cannot be done precisely. Laborious iterative algorithms must be used for the inversion, calculations impractical until the advent of modern digital computers. For this reason, Drude and, later, Tronstad developed approximate expressions for the quantities Δ-$\overline{\Delta}$ and ψ-$\overline{\psi}$ which were linear in film thickness, d, but accurate only for very thin films ($d << \lambda$). Here, the bar indicates the parameters for the film-free case of Section 2.6.1. For certain instances, Burge and Bennett (Ref. 29) report large discrepancies between the optical parameter values determined from the approximate relations and those determined from Eq. (69). Most present-day investigators make use of computer algorithms for obtaining the desired parameters from Eq. (69). The algorithms vary according to the parameters sought, the information known, and the criteria for convergence.

In principle, all nine parameters can be determined if at least nine independent ellipsometric measurements are made. However, in nearly all cases, the parameters ν, ϕ_0, and $\hat{n}_o$, the ambient refractive index, are known. Of the remaining five parameters, the substrate complex refractive index $\hat{n}_2 = n_2 + ik_2$ is often also obtained from previous measurements, leaving just the three film parameters n_1, k_1, and thickness, d, to be determined. In a typical ellipsometric experiment, only two quantities are measured, a single value of ψ and one of Δ. Thus, unless the film is known to be nonabsorbing or unless its thickness is known, the three unknown film parameters cannot be found from a single typical ellipsometer run, and additional information must be sought.

2.6.2.1 Case of Only Two Unknown Parameters

If only two of the original nine parameters in the ambient-thin film-substrate system are unknown, the unknown parameters may be determined from a measured ψ value and a measured Δ value. In principle, any two of the nine parameters may be unknown, but frequently the two unknowns are: (1) n_1 and d of a transparent film, (2) n_1 and k_1 of an absorbing film, or (3) the optical constants n_2 and k_2 of the substrate.

Several authors (Refs. 30 and 31) have written algorithms appropriate for cases 1 and 2 above. McCrackin (Ref. 30) describes a FORTRAN program that will compute the two unknown parameters, either n_1 or k_1, or n_1 and d_1, from the ellipsometer settings of the polarizer and analyzer angles, P and A. The program corrects for differences in the attenuation of the fast and slow components of a beam passing through an imperfect compensator (Section 2.4.3), and misalignment of the sample surfaces.

2.6.2.2 Case of Three or More Unknown Parameters

If three or more parameters (e.g., n_1, k_1, and d of an absorbing film) are to be determined from ellipsometric measurements, it may be possible to obtain sufficient independent observations of ψ and Δ by varying either (1) the film thickness, d, (2) the ambient medium, $\hat{n}_0$, (3) the substrate medium, $\hat{n}_2$, (4) the angle of incidence, ϕ_0 (multiple angle of incidence (MAI) ellipsometry), (5) the film material, $\hat{n}_1$, or (6) any given combination of d, $\hat{n}_0$, $\hat{n}_1$, $\hat{n}_2$, and ϕ_0. McCrackin and Colson (Ref. 32) have studied applications of schemes 1 through 4 to find the three absorbing film parameters n_1, k_1, and d. They concluded that because of experimental uncertainties the variation of film thickness method — method 1 — works only for film thicknesses greater than about 0.010 μm, even if n_1 and k_1 are assumed to not change with thickness. They found that the methods employing different ambients or substrates (methods 2 and 3) were most likely to yield unique film parameters. Of these two methods, method 2 — the variation of the ambient (usually a fluid) — would ordinarily be easier to apply than method 3 because of the difficulty inherent to method 3 of depositing identical films on different substrates.

Several authors have discussed multiple angle of incidence (MAI) ellipsometry, method 4 above (Ref. 33). Azzam and Bashara (Ref. 4) provide general criteria for choosing the angles of incidence and the least-squares converging function to be minimized if the number of independently measured quantities exceeds the number of unknown parameters. For a simulated SiO film on a Si substrate in which five parameters (n_1, k_1, d, n_2, and k_2) were found by the least-squares algorithm of Marquardt (Ref. 34), Azzam and Bashara noted more rapid convergence for very thin films ($< 0.010\,\mu$m) than for thicker films ($> 0.10\,\mu$m). They also concluded that for all film thicknesses, convergence to the proper parameter

values failed unless fairly accurate (± 15 percent) initial estimates of the parameter values were used.

To date, we have not seen any analyses of ellipsometric schemes in which a given combination of the parameters ϕ_o, d, $\hat{n}_o$, $\hat{n}_1$, and $\hat{n}_2$ is allowed to vary. In principle, at least, such schemes utilizing Marquardt's algorithm (Ref. 34) are possible and show promise for future applications.

Additional information may come from non-ellipsometric methods. For example, in the case of IR ellipsometric measurements of an unknown absorbing thin film, the method of Templemeyer and Mills (Ref. 35) may be used for an independent measurement of film thickness, and the parameters n_1 and k_1 may be found from a single measurement of ψ and one of Δ.

2.7 COMMERCIALLY AVAILABLE ELLIPSOMETRIC INSTRUMENTATION

The two major suppliers of ellipsometric equipment are Rudolph Research and Gaertner Scientific Corporation. Both manufacturers offer the two styles of ellipsometers listed in Table 1: (1) production models that can be fully automated and (2) research instruments that can be used to make more precise measurements and that can be partially automated with optional components. The accessories and warranties offered by both firms are essentially the same. All commercially available ellipsometers are in the PCSA configuration.

Table 1. Commercially Available Ellipsometers

Ellipsometer Type	Gaertner	Rudolph Research
Production Manual	L117	RR100
Automatic	L116	AutoEL-II and AutoEL-III
Research	L118GT (0.1-deg Precision) L119 (0.01-deg Precision)	436 (Vertical Sample) 437 (Horizontal Sample)

2.7.1 Commercially Produced Ellipsometers

The production ellipsometers are designed for easy and fast measurements of the thickness, d, and refractive index, n_1, of a thin transparent film on a known substrate, and at the He-Ne laser wavelength of 0.6328 μm. The two or three allowed angles of incidence are usually pin adjustable. The automatic models achieve rapid response either with a continuously rotating analyzer or with stepper-motor-driven polarizers and analyzers (Ref. 36). This allows the use of a programmable calculator to compute ψ and Δ, and, often, n_1 and d. The production ellipsometers are not designed for measurements of sample systems enclosed in environmental chambers but can accommodate liquid sample systems on their standard horizontal mounts.

Both manufacturers supply optional optics that can reduce the beam cross-sectional diameter to 26 μm. This allows a high-resolution mapping of film thickness across a horizontally mounted substrate. Indeed, the Gaertner L115 system includes an L116 ellipsometer and associated electronics that can automatically provide a hard copy mapping of thin-film thickness over a predetermined area of a substrate.

The Gaertner L116 automatic production ellipsometer is essentially an L117 manual production ellipsometer with a rotating analyzer. (See Section 2.4.5.) The angles of incidence can be 30, 50, or 70 degrees. A Hewlett-Packard HP9825 calculator can process the ellipsometric measurements to find the index of refraction, n_1, and the thickness, d, of a nonabsorbing film on a known substrate. The calculator can also control optional stepper-motor-driven scanning stages for the sample that allow different sampling points anywhere within a 5-in.-diam area on the sample. Provisions have just become available for adding the new programs to the calculator for multiple transparent films and for absorbing films. In addition to having the L116 with HP9825 and the motor-driven scanning stages, the L115 system also has a Hewlett-Packard HP7225A plotter to permit a graphical display of thickness scans. The optics for beam size reduction must be factory installed on all Gaertner production models and are not removable.

The AutoEL series of ellipsometers given in Table 1 comprises the automatic production models built by Rudolph Research. A manual production model, RR100, is also built by Rudolph Research, but it is less accurate. The AutoEL ellipsometers are null-seeking (Section 2.4.3) and use a microcomputer to drive stepper motors to select the proper polarizer and analyzer settings. The AutoEL-III ellipsometer is a more advanced version of the lower-priced AutoEL-II, but both achieve the measuring accuracies of the Gaertner L116 and L117 models. The AutoEL-II is designed primarily for automatic measurement of the index of refraction, n_1, and the thickness, d, of a thin transparent film on a known

substrate. The AutoEL-III has the added capabilities of an accessible computer memory and can find the thicknesses and the refractive indices of a double layer of nonabsorbing films or the optical constants of bare absorbing substrates. Other computer programs may be added to the AutoEL series.

In the Rudolph Research AutoEL series of ellipsometers, the optional translatable sample stages are manually adjustable, as opposed to the (optional) motor-driven stages for the Gaertner L116 ellipsometer. However, the beam reduction optics of the AutoEL series are removable, and the angles of incidence may be pin-locatable or set with alignment prisms. The customer may specify any set of two or three incident angles between 60 and 90 deg for either pin-set or prism-set angles.

2.7.2 Commercial Research Ellipsometers

The research ellipsometers from Gaertner are the L118GT and L119 models (Table 1). These are basically modified spectrometers (Ref. 13) with *vertical* substrate mounts which can be translated as well as rotated. An optional support for the entire ellipsometer to accommodate *horizontal* samples (e.g., liquid) is available; however, the ellipsometer must be modified at the factory. Component settings can be read to within 0.1 deg on the L118GT and to within 0.01 deg on the L119. The minimum angle of incidence of both models is 22.5 deg. The standard ellipsometer components are manually adjusted, but an optional rotating analyzer is available for either model. Light sources (e.g., He-Ne lasers, or mercury lamps with filters), a Babinet-Soleil compensator, and detectors are also optional items.

The L119X ellipsometer is the large based version of the L119 which will allow the use of environmental chambers surrounding the sample, which must be mounted vertically. Factory-installed beam reduction optics (to 26 μm diameter) are available only for the L119X. Extended spectral range measurements (from 0.215 to 3 μm) can be made with the L119XUV, an L119X model with non-glass optics.

The 436 research ellipsometer for vertically mounted samples from Rudolph Research has the measuring precision of the Gaertner L119. The Rudolph Research 437 model is a sturdier version of the 436 ellipsometer. The 437 is designed for horizontally mounted samples. The models are identical in all respects other than ranges of the angle of incidence, which are 25 to 90 degrees for the 436 and 50 to 90 degrees for the 437. Because nearly all ellipsometric measurements are made at angles of incidence near the principal angle, Θ, which is usually about 70 deg (Section 2.4.4), the more restricted incidence angle range of the 437 would present a problen only rarely, even in multiple angle of incidence (MAI) ellipsometry (Ref. 4). A mercury light source, filters, apertures, sample holder, and a

photomultiplier tube (PMT) light detection system are supplied as standard equipment on the 436 and 437. These items are optional for the Gaertner research ellipsometers.

The optional items for the Rudolph Research research ellipsometers include He-Ne laser and stabilized tungsten-iodine sources, Babinet-Soleil compensators, rotating analyzers, and digital readout rotators for the polarizer and analyzer. The rotating analyzer provides faster measurements but is less accurate and requires more frequent maintenance than the manually adjusted analyzers. Environmental chambers can be used with the 436 and 437 if the optical components of the ellipsometer are mounted on optional optical benches; thus it is not necessary to buy a special model for environmental chambers, which is the case for the Gaertner line of research ellipsometers. Beam size reduction optics are also available that can produce a beam diameter of 2.5 μm, one-tenth the size of the smallest diameter available for the corresponding Gaertner optics.

2.7.3 Recommendations Concerning Ellipsometric Equipment

The limitations of commercial production ellipsometers must be considered when choosing between a production ellipsometer and a research ellipsometer. These limitations are

1. The production instruments are less accurate but faster and easier to use.
2. All measurements must be at 0.6328 μm and are restricted to a few fixed angles of incidence.
3. There are more restrictions in the choice of sample systems that can be analyzed by production instruments, but complete data analysis systems are available for them.
4. No environmental chamber measurements can be made with production ellipsometers.

If the AEDC chooses a production ellipsometer, we recommend that the Gaertner L117 manual production ellipsometer be selected. We base our choice partly on the assumption that speed of measurement is not important. The L117 can be factory-fitted with beam reduction optics and sample-positioning devices; also, all of the data reduction capabilities of the Gaertner L116 automatic production ellipsometer are available.

However, if an automatic production ellipsometer is desired at the outset, we recommend the Rudolph Research AutoEL-III over the comparably priced Gaertner L116 system. The flexibility of the AutoEL-III is slightly greater than that of the Gaertner L116

(e.g., the AutoEL-III has user-removable beam reduction optics) which would probably offset the faster data analysis time claimed by Gaertner for the L116. [The analysis times for a single film are given as four seconds for the L116 (Ref. 37) and 15 seconds for the AutoEL-III (Ref. 38).] We would recommend the much more expensive Gaertner L115 system only for the case requiring profiles of film thickness on a substrate.

The authors strongly recommend the Rudolph Research 436 or 437 research instruments if the AEDC is to acquire a research ellipsometer. In fact, unless the AEDC has firm plans to never measure liquid samples, we feel that a 437 should be purchased because of its sturdier construction.

While the Gaertner L119 research ellipsometer offers the same capabilities as either the Rudolph Research 436 or 437, changes in ellipsometer configurations are more awkward and time-consuming for the L119 model. For instance, versions of the L119 that can measure horizontally mounted samples or those that can accommodate environmental sample chambers must be assembled at the factory. In contrast, the 437 is designed especially for horizontal samples (of both liquids and solids), and either the 436 or the 437 can be converted to vacuum instruments by the user, with use of optional optical benches. Furthermore, there is no stock version of the L119 available that can rival the versatility of the 437 with its optical benches that can measure horizontally mounted samples in an environmental chamber.

2.8 SUMMARY ON ELLIPSOMETRY

In the near-IR to near-UV spectral region, ellipsometric methods are comparable, or superior, to conventional transmission and reflection spectroscopic techniques for obtaining both the optical constants of thin films and substrates and the thicknesses of films. The wide variety of ellipsometric instrument configurations creates a myriad of analysis schemes, not all of which have been explored. The possibilities of making ellipsometric measurements in the IR are being explored by a number of researchers; these measurements could be made if existing commercial ellipsometers were modified.

Only PSCA ellipsometers are commercially available, and these are of two types, production and research. The less accurate production ellipsometers can be fully automated to determine the optical parameters of simple systems, but only at a wavelength of 0.6328 μm. With optional optics, the manual research ellipsometers can operate in the spectral region from 0.210 to about 3 μm. The commercial ellipsometers rated best by the authors are: (1) the Gaertner L117 manual production ellipsometer, (2) the Rudolph Research AutoEL-III automatic production ellipsometer, and (3) the Rudolph Research 437 research ellipsometer.

3.0 INTERNAL REFLECTION SPECTROSCOPY (IRS) OF FILMS

In most ellipsometric measurements (Section 2.0) or conventional reflectance experiments, a refracted ray moving away from an interface of two media removes part of the power of the incident beam that would otherwise go to the reflected beam. However, if the two media are transparent and the incident beam is in the medium of the higher refractive index, then a beam incident at angles greater than a specific "critical" angle will not cause a refracted beam to appear in the lower index medium, and the incident and reflected beams will have equal power. This well-known phenomenon is termed total internal reflection (TIR) or simply total reflection. The word "internal" is usually applied because total reflection is often seen when the incident beam is in glass or water and the incident medium is surrounded by or has a boundary with the ambient air.

Issac Newton noticed that when a beam undergoing total reflection is within a glass prism, a second prism brought sufficiently close to the first (but not in contact) will cause propagation of light within the second prism and a corresponding reduction in the reflected beam intensity in the first prism. This is known as frustrated total reflection (FTR) energy coupling, and is useful in the precise measurement of small distances (Ref. 39). FTR coupling clearly indicates that an electromagnetic field (the "evanescent" field or wave) exists in the rarer (lower refractive index) medium even under the conditions of total reflection. However, because the intensities of the totally reflected beam and the incident beam are equal, it must be true that the time average energy of the evanescent wave must be zero. (See Section 3.1.)

Another method for "frustrating" total reflection is to replace the rarer *transparent* medium with a rarer *absorbing* medium. Here, the dipole interaction of the evanescent wave with the molecules of the rarer medium causes a loss in the power of the reflected beam. This energy coupling process, called attenuated total reflection (ATR), reveals molecular absorption spectra very similar to transmission spectra, and forms the basis for internal reflection spectroscopy (IRS).

The research of Fahrenfort (Ref. 40) and Harrick (Ref. 41) began the present interest in IRS methods. Their work showed that IRS was more sensitive than conventional reflection methods, especially for weaker absorptions. Harrick's text (Ref. 42) describes the theory of IRS and its numerous applications, and has become the standard authority on internal reflection spectroscopy.

Unlike ellipsometry, IRS techniques can be readily applied to measurements throughout the IR spectral region. Other attributes include (Ref. 43): (1) enhanced sensitivity to the

optical constants of materials over other reflectance methods; (2) the ability to selectively test the optical thickness of very thin films and surface states because of the small penetration depth of the evanescent wave; (3) the low light loss per reflection for nonabsorbing samples, thereby making multiple reflection techniques feasible even for very thin films; and (4) the determination of the orientations of molecules at a surface.

3.1 THEORY OF TOTAL REFLECTION AT THE INTERFACE OF TWO SEMI-INFINITE MEDIA

From Maxwell's laws of electromagnetism one may show that at the interface of two media, the normal components of both the magnetic induction field, $\vec{B}$, and the electric displacement field, $\vec{D} = \hat{n}^2 \vec{E}$, are the same on either side of the boundary (Ref. 25). The Fresnel relations, Eqs. (58) through (61), follow from these boundary conditions as well as from Snell's law.

In general, Snell's law concerning the angles made by the incident and refracted beams to the normal of an interface of two media of complex indices of refraction, $\hat{n}_i$ and $\hat{n}_j$, may be written

$$\hat{n}_i \sin \hat{\Phi}_i = \hat{n}_j \sin \hat{\Phi}_j \tag{70}$$

For two absorbing media the complex arguments Φ_i and Φ_j have complicated relationships with the angles of incidence and refraction. Even if the two media are transparent, the argument corresponding to the smaller (real) index of refraction must be complex for conditions in which its sine function value is greater than unity.

First the simpler case of total reflection at the interface of two semi-infinite transparent media will be considered. Then the effects caused by replacing the rarer transparent medium with a rarer absorbing one will be discussed.

3.1.1 Total Reflection for Two Transparent Media

For the two semi-infinite transparent media shown in Fig. 8, Snell's law [Eq. (70)] is

$$n_1 \sin \phi_1 = n_2 \sin \hat{\Phi}_2 \tag{71}$$

The argument $\hat{\Phi}_2$ is real (and equals $\phi_2 > \phi$) only if $\phi_1 \leq \phi_{12c}$, the critical angle for transparent media 1 and 2. The critical angle, ϕ_{12c}, is the value of ϕ_1 corresponding to $\phi_2 = \pi/2$, so

$$\phi_{12c} = \sin^{-1}(n_2/n_1) = \sin^{-1} n_{21} \tag{72}$$

where n_{21} is the relative refractive index for media 1 and 2 and is defined as

$$n_{21} \equiv n_2/n_1 \tag{73}$$

If $\phi_1 > \phi_{12c}$, then ϕ_2 has no physical significance, and total reflection occurs at the interface if the incident beam is in the denser medium, n_1. (Note that if the incident beam is in the rarer medium, n_2, then ϕ_2 is always less than or equal to $\pi/2$ and ϕ_1 can never be greater than ϕ_{12c}.)

3.1.1.1 Representation of the Electric Fields

The electric fields of the incident, reflected, and refracted beams are represented in Fig. 8 by the vectors $\vec{E}$, $\vec{R}$, and $\vec{T}$, respectively. From the orientations of the vectors pictured in Fig. 8 and adopting the notation appearing in Eqs. (1), (2), (3), (11), and (12), we may write

$$\vec{E} = \mathrm{Re}\left\{\left[\left(\vec{u}_x \cos\phi_1 - \vec{u}_z \sin\phi_1\right)E_{po}\, e^{-i\alpha_p} + \vec{u}_y E_{so}\, e^{-i\alpha_s}\right] \cdot \exp\left\{-i\omega\left[t - \frac{n_1}{c}(x \sin\phi_1 + z\cos\phi_1)\right]\right\}\right\} \tag{74}$$

$$\vec{R} = \mathrm{Re}\left\{\left[-\left(\vec{u}_x \cos\phi_1 + \vec{u}_z \sin\phi_1\right)R_{po}\, e^{-i\beta_p} + \vec{u}_y R_{so}\, e^{i\beta_s}\right] \cdot \exp\left\{-i\omega\left[t - \frac{n_1}{c}(x \sin\phi_1 - z\cos\phi_1)\right]\right\}\right\} \tag{75}$$

and

$$\vec{T} = \mathrm{Re}\left\{\left[\left(\vec{u}_x \cos\hat{\Phi}_2 - \vec{u}_z \sin\hat{\Phi}_2\right)T_{po}\, e^{-i\xi_p} + \vec{u}_y T_{so}\, e^{-i\xi_s}\right] \cdot \exp\left\{-i\omega\left[t - \frac{n_2}{c}(x \sin\hat{\Phi}_2 + z\cos\hat{\Phi}_2\right]\right\}\right\} \tag{76}$$

In the above equations, $\vec{u}_l$ (for l = x, y, or z) refers to the unit vectors along the corresponding axis directions pictured in Fig. 8. That is, the z-axis is directed normally into the rarer medium, n_2, at the point of incidence on the interface, and the x-axis lies along the interface in the plane of incidence. $\hat{\Phi}_2$ is real (and equals ϕ_2) only if ϕ_1 is less than the critical angle, ϕ_{12c}.

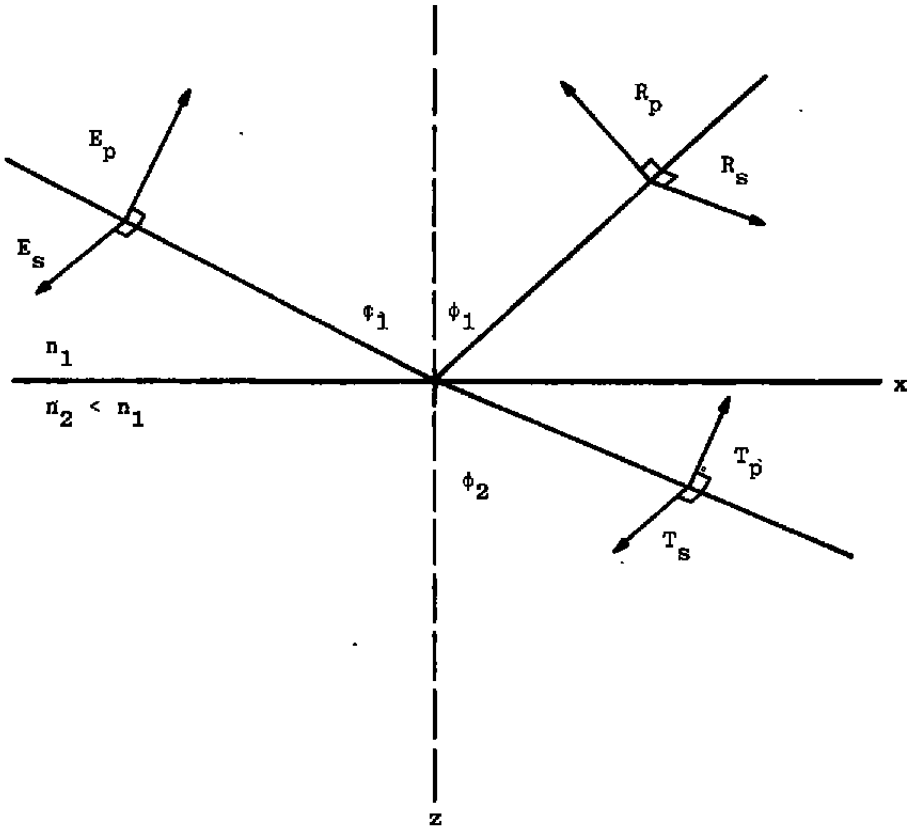

Figure 8. Parallel and perpendicular components of the electric field of the incident ($\vec{E}$), reflected ($\vec{R}$), and refracted ($\vec{T}$) beams at the interface of two transparent media when the incident beam is in the optically denser medium.

3.1.1.2 The Fresnel Relations

The amplitudes E_{po}, E_{so}, R_{po}, R_{so}, T_{po}, and T_{so} in Eqs. (74), (75), and (76) are real and constant under steady-state conditions. It is convenient to define corresponding constant complex amplitudes as follows:

$$\hat{E}_{\parallel} \equiv E_{po}\, e^{-i\alpha_p} \qquad \hat{R}_{\perp} \equiv R_{so}\, e^{-i\beta_s}$$

$$\hat{E}_{\perp} \equiv E_{so}\, e^{-i\alpha_s} \qquad \hat{T}_{\parallel} \equiv T_{po}\, e^{-i\xi_p}$$

$$\hat{R}_{\parallel} \equiv R_{po}\, e^{-i\beta_p} \qquad \text{and} \qquad \hat{T}_{\perp} \equiv T_{so}\, e^{-i\xi_s} \tag{77}$$

The Fresnel relations are obtained by matching electric field components on either side of the interface at the point of incidence (x = y = z = o). From Eqs. (74) through (77), we see that the transmission and reflection coefficients are simply the ratios of the complex amplitudes because the time dependences in Eqs. (74) through (76) are identical at the origin of the x-y-z coordinate system, the point of incidence. Thus, when Snell's law, Eq. (72), and Eq. (77) are put into Fresnel's relations, [Eqs. (58) through (61)], the modified Fresnel relationships result:

$$\hat{r}_{12p} = \frac{\hat{R}_{\|}}{\hat{E}_{\|}} = \frac{\tan(\phi_1 - \hat{\Phi}_2)}{\tan(\phi_1 + \hat{\Phi}_2)} = \frac{\sin\phi_1 \cos\phi_1 - \sin\hat{\Phi}_2 \cos\hat{\Phi}_2}{\sin\phi_1 \cos\phi_1 + \sin\hat{\Phi}_2 \cos\hat{\Phi}_2} \tag{78}$$

$$\hat{r}_{12s} = \frac{\hat{R}_{\perp}}{\hat{E}_{\perp}} = \frac{-\sin(\phi_1 - \hat{\Phi}_2)}{\sin(\phi_1 + \hat{\Phi}_2)} = \frac{\sin\phi_1 \cos\hat{\Phi}_2 - \cos\phi_1 \sin\hat{\Phi}_2}{\sin\phi_1 \cos\hat{\Phi}_2 + \cos\phi_1 \sin\hat{\Phi}_2} \tag{79}$$

$$\hat{t}_{12p} = \frac{\hat{T}_{\|}}{\hat{E}_{\|}} = \frac{2\cos\phi_1 \sin\hat{\Phi}_2}{\sin(\phi_1 + \hat{\Phi}_2)\cos(\phi_1 - \hat{\Phi}_2)} = \frac{2\cos\phi_1 \sin\hat{\Phi}_2}{\sin\phi_1 \cos\phi_1 + \sin\hat{\Phi}_2 \cos\hat{\Phi}_2} \tag{80}$$

and

$$\hat{t}_{12s} = \frac{\hat{T}_{\perp}}{\hat{E}_{\perp}} = \frac{2\cos\phi_1 \sin\hat{\Phi}_2}{\sin(\phi_1 + \hat{\Phi}_2)} = \frac{2\cos\phi_1 \sin\hat{\Phi}_2}{\sin\phi_1 \cos\hat{\Phi}_2 + \sin\hat{\Phi}_2 \cos\phi_1} \tag{81}$$

The Fresnel relations involving sums or differences of ϕ_1 and $\hat{\Phi}_2$ are given by Born and Wolf (Ref. 25).

3.1.1.3 The Energy Conditions of Total Reflection

Total reflection of a beam can be shown to occur at the interface of two transparent media when the angle of incidence, ϕ_1, exceeds the critical angle, ϕ_{12c}; i.e., all the power of the incident beam appears in the reflected beam when $\phi_1 > \phi_{12c}$.

When $\phi_1 > \phi_{12c}$, Eq. (72) gives

$$\sin\hat{\Phi}_2 = \sin\phi_1/n_{21} > 1 \tag{82}$$

Thus,

$$\cos\hat{\Phi}_2 = \left[1 - \sin^2\hat{\Phi}_2\right]^{1/2} = i\left[\sin^2\hat{\Phi}_2 - 1\right]^{1/2}$$

$$= i\left[\frac{\sin^2\phi_1}{n_{21}^2} - 1\right]^{1/2} \tag{83}$$

The positive square root in Eq. (83) must be chosen so that the electric field will not appear to increase exponentially with z in the rarer medium. Substituting Eqs. (82) and (83) into the last relation presented in each of Eqs. (78) through (81), produces, for $\phi_1 > \phi_{12c}$,

$$\hat{r}_{12p} = \frac{n_{21}^2 \cos\phi_1 - i\left[\sin^2\phi_1 - n_{21}^2\right]^{1/2}}{n_{21}^2 \cos\phi_1 + i\left[\sin^2\phi_1 - n_{21}^2\right]^{1/2}} \tag{84}$$

$$\hat{r}_{12s} = \frac{\cos\phi_1 - i\left[\sin^2\phi_1 - n_{21}^2\right]^{1/2}}{\cos\phi_1 + i\left[\sin^2\phi_1 - n_{21}^2\right]^{1/2}} \tag{85}$$

$$\hat{t}_{12p} = \frac{2n_{21}\cos\phi_1}{n_{21}^2\cos\phi_1 + i\left[\sin^2\phi_1 - n_{21}^2\right]^{1/2}} \tag{86}$$

and

$$\hat{t}_{12s} = \frac{2\cos\phi_1}{\cos\phi_1 + i\left[\sin^2\phi_1 - n_{21}^2\right]^{1/2}} \tag{87}$$

The magnitudes of the denominators and numerators of both Eqs. (84) and (85) are identical, giving

$$\left|\hat{r}_{12p}\right|^2 = 1 \tag{88}$$

and

$$\left|\hat{r}_{12s}\right|^2 = 1 \tag{89}$$

That is, all of the intensity of the parallel component of the incident beam appears in the parallel component of the reflected beam when $\phi > \phi_{12c}$, and likewise for the perpendicular components.

3.1.1.4 Phase Shifts Upon Reflection

For total reflection, the expressions for $\hat{r}_{12p}$ and $\hat{r}_{12s}$ can be written [Eqs. (77), (78), (79), (88), and (89)] as

$$\hat{r}_{12\ell} = \left|\hat{r}_{12\ell}\right| e^{-i(\beta_\ell - \alpha_\ell)} = e^{-i\delta_\ell} \; ; \; \ell = p, s \tag{90}$$

where

$$\delta_\ell = \beta_\ell - \alpha_\ell \tag{91}$$

The form of $\hat{r}_{12\ell}$ is shown in Eqs. (84), (85), (90), and (91) to be

$$\hat{r}_{12\ell} = \frac{a_\ell - ib}{a_\ell + ib} = e^{-2ig_\ell} \tag{92}$$

where

$$\tan g_\ell = \tan \frac{\delta_\ell}{2} = \frac{b_\ell}{a_\ell} \quad ; \quad \ell = p, s \tag{93}$$

The combination of Eqs. (84) and (85) with (92) and (93) yields

$$\tan \frac{\delta_p}{2} = \frac{-\left[\sin^2 \phi_1 - n_{21}^2\right]^{1/2}}{n_{21}^2 \cos \phi_1} \tag{94}$$

and

$$\tan \frac{\delta_s}{2} = \frac{-\left[\sin^2 \phi_1 - n_{21}^2\right]^{1/2}}{\cos \phi_1} \tag{95}$$

Therefore, the changes in polarization at total reflection are not the same for each component, and, in general, the reflected beam is elliptically polarized even if the incident beam is plane polarized.

It is interesting to see what the ellipsometric parameters ψ and $\Delta = \delta_p - \delta_s$ become under the conditions of total reflection for two semi-infinite transparent media (Section 2.0). From Eq. (11),

$$\hat{\rho} = \frac{\hat{r}_{12p}}{\hat{r}_{12s}} = e^{-i\Delta} \tag{96}$$

which upon comparison with Eqs. (12), (94), and (95) gives

$$\tan \psi = 1 \tag{97}$$

and

$$\tan\frac{\Delta}{2} = \frac{\tan\frac{\delta_p}{2} - \tan\frac{\delta_s}{2}}{1 + \tan\frac{\delta_p}{2}\tan\frac{\delta_s}{2}} = \frac{\cos\phi_1\left[\sin^2\phi_1 - n_{21}^2\right]^{1/2}}{\sin^2\phi_1} \tag{98}$$

So, for ellipsometric measurements of two semi-infinite transparent media under the conditions of total reflection, ψ is already determined from Eq. (97) to be $\pi/4$ plus an integer multiple of π, and only Δ needs to be found. The relative index can be calculated from Eq. (98).

3.1.1.5 The Nature of the Evanescent Field

One may evaluate Eqs. (86) and (87) for $|\hat{t}_{12p}|^2$ and $|\hat{t}_{12s}|^2$ and see that neither quantity is zero, which indicates that some power must enter the rarer medium, forming the evanescent field. If the time average power in the rarer medium is computed, however, one finds it is zero (Ref. 25), and the evanescent field has the form of a standing wave (Ref. 46).

The form of the evanescent wave is evident when, in Eq. (76), $\sin\hat{\Phi}_2$ and $\cos\hat{\Phi}_2$ are replaced by the expressions given in Eqs. (82) and (83):

$$\vec{T} = \mathrm{Re}\left\{\left[\vec{u}_x\,\vec{T}_x + \vec{u}_y\,\vec{T}_y + \vec{u}_z\,\vec{T}_z\right]\exp\left[-\frac{n_2\,\omega z}{c}\left(\frac{\sin^2\phi_1}{n_{21}^2} - 1\right)^{1/2}\right]\right.$$

$$\left.\cdot\exp\left[-i\omega\left(t - \frac{n_1\sin\phi_1}{c}\,x\right)\right]\right\}$$

$$= \mathrm{Re}\left\{\vec{u}\,\hat{T}_o\,e^{-z/d_p}\,e^{-i\theta_t}\right\} \tag{99}$$

where

$$\hat{T}_x = \hat{T}_{\parallel}\cos\hat{\Phi}_2 = i\left[\frac{\sin^2\Phi_1}{n_{21}^2} - 1\right]^{1/2}\hat{T}_{\parallel} \tag{100}$$

$$\hat{T}_y = \hat{T}_{\perp} \tag{101}$$

$$\hat{T}_z = -\hat{T}_{\parallel} \sin \hat{\Phi}_2 = -\frac{\sin \phi_1}{n_{21}} \hat{T}_{\parallel} \tag{102}$$

$$\vec{u}\,\hat{T}_o \equiv \vec{u}_x \hat{T}_x + \vec{u}_y \hat{T}_y + \vec{u}_z \hat{T}_z \tag{103}$$

$$\theta_t \equiv \omega \left[t - \frac{n_1 \sin \phi_1 \, x}{c} \right] \tag{104}$$

and the "penetration depth," d_p, is (Ref. 44)

$$d_p = \frac{c}{\omega n_1 \left[\frac{\sin^2 \phi_1}{n_{21}^2} - 1 \right]^{1/2}} = \left[2 \pi \nu n_1 \left(\sin^2 \phi_1 - n_{21}^2 \right)^{1/2} \right]^{-1} \tag{105}$$

Equation (99) is that of a periodic disturbance that is propagating in the rarer medium along the interface in the plane of incidence (the x-direction), and whose amplitude experiences an exponential decay along the normal away from the interface (the z-direction).

The penetration depth is, then, infinite at the critical angle $\phi_{12C} = \sin^{-1} n_{21}$. The smallest value of d_p is at grazing incidence ($\phi_1 = \pi/2$), and we can estimate its value by examining Eq. (105) at $\phi_1 = \pi/2$ and for very small n_{21}. We have

$$\lim_{n_{21} \to o} d_p \, (\phi_1 = \pi/2) = (2 \pi \nu n_1)^{-1} = \frac{\lambda}{2 \pi n_1} \tag{106}$$

So, for two transparent media, the depth of penetration can be anywhere from a fraction, $(2\pi)^{-1}$, of the wavelength in the dense medium (λ/n_1) to infinite; hence, it is possible to selectively sample a thin layer in multiple-layer films. Also note that at a fixed angle of incidence, the penetration depth increases with wavelength.

Correspondingly, a consideration of absorbing media requires knowledge of the relative magnitudes of the transmitted electric fields very near the interface. Expressions are derived herein for those quantities.

If Eqs. (80), (81), (86), and (87) are combined with Eqs. (100) through (102), we may write

$$\frac{\hat{T}_x}{\hat{E}_{\parallel}} = \hat{t}_{12p}\, i \sqrt{\frac{\sin^2 \phi_1}{n_{21}^2} - 1}$$

$$= \frac{2\, i \cos \phi_1 \sqrt{\sin^2 \phi_1 - n_{21}^2}}{n_{21}^2 \cos \phi_1 + i \sqrt{\sin^2 \phi_1 - n_{21}^2}} \tag{107}$$

$$\frac{\hat{T}_y}{\hat{E}_{\perp}} = \hat{t}_{12s} = \frac{2 \cos \phi_1}{\cos \phi_1 + i \sqrt{\sin^2 \phi_1 - n_{21}^2}} \tag{108}$$

and

$$\frac{\hat{T}_z}{\hat{E}_{\parallel}} = -\hat{t}_{12p} \left(\frac{\sin \phi_1}{n_{21}} \right)$$

$$= -\frac{2 \cos \phi_1 \left(\frac{\sin \phi_1}{n_{21}} \right)}{\cos \phi_1 + i \sqrt{\sin^2 \phi_1 - n_{21}^2}} \tag{109}$$

This gives the amplitude ratios at the boundary as

$$\left| \frac{\hat{T}_x}{\hat{E}_{\parallel}} \right| = \frac{2 \cos \phi_1 \sqrt{\sin^2 \phi_1 - n_{21}^2}}{\left\{ \left(1 - n_{21}^2 \right) \left(\sin^2 \phi_1 - n_{21}^2 \cos^2 \phi_1 \right) \right\}^{1/2}} \tag{110}$$

$$\left| \frac{\hat{T}_y}{\hat{E}_{\perp}} \right| = \frac{2 \cos \phi_1}{\sqrt{1 - n_{21}^2}} = \left| \frac{\hat{T}_{\perp}}{\hat{E}_{\perp}} \right| \tag{111}$$

and

$$\left| \frac{\hat{T}_z}{\hat{E}_{\parallel}} \right| = \frac{2 \sin \phi_1 \cos \phi_1}{\left\{ \left(1 - n_{21}^2 \right) \left(\sin^2 \phi_1 - n_{21}^2 \cos^2 \phi_1 \right) \right\}^{1/2}} \tag{112}$$

Also,

$$\left|\frac{\hat{T}_{\parallel}}{\hat{E}_{\parallel}}\right| = \left(\left|\frac{\hat{T}_x}{\hat{E}_{\parallel}}\right|^2 + \left|\frac{\hat{T}_z}{\hat{E}_{\parallel}}\right|^2\right)^{1/2}$$

$$= \frac{2\cos\phi_1\left(2\sin^2\phi_1 - n_{21}^2\right)^{1/2}}{\left\{\left(1 - n_{21}^2\right)\left(\sin^2\phi_1 - n_{21}^2\cos^2\phi_1\right)\right\}^{1/2}} \tag{113}$$

The factor of 2 in each of these four relations indicates that the evanescent field is in the form of a standing wave (Ref. 44).

3.1.2 Attenuated Total Reflection for a Semi-Infinite Transparent Dense Medium and a Semi-Infinite Absorbing Medium

If the transparent rarer medium of the last section is replaced by a semi-infinite absorbing rarer medium, there is energy coupling (ATR) by the incident beam with the evanescent field in the rarer medium when the incident angle exceeds the critical angle. Actually, because of the limited extent of the evanescent wave into the rarer medium, it is usually unnecessary to experimentally approximate a semi-infinite with a large block of rarer material volume. A thick film of the rarer medium will suffice if its thickness, d, is much greater than the penetration depth, d_p.

In the case of an absorbing rarer medium, with complex index of refraction $\hat{n}_2 = n_2 + ik_2$, the critical angle, ϕ_{12c}, is not given by Eq. (72) because $\hat{n}_2$ is not real. Furthermore, the amplitude of a wave propagating within an absorbing medium depends on the distance it travels within the medium.

Internal reflection measurements of the attentuated total reflection processes at the interface of a transparent medium (with an index of refraction $\hat{n}_1 = n_1$) and an absorbing medium (with a complex refractive index of $\hat{n}_2 = n_2 + ik_2$) can be interpreted from the complex Fresnel relations [Eqs. (58) through (61)] when modified by Snell's law [Eq. (70)] and complex arguments. Thus, at the interface of media i and j,

$$\cos\Phi_j = \sqrt{1 - \sin^2\hat{\Phi}_j} = \sqrt{1 - (\hat{n}_i/\hat{n}_j)^2\sin^2\hat{\Phi}_i} \tag{114}$$

the complex Fresnel-Snell relations are

$$\hat{r}_{ijp} = \frac{\hat{n}_i \sqrt{1 - (\hat{n}_i/\hat{n}_j)^2 \sin^2 \hat{\Phi}_i} - \hat{n}_j \cos \hat{\Phi}_i}{\hat{n}_i \sqrt{1 - (\hat{n}_i/\hat{n}_j)^2 \sin^2 \hat{\Phi}_i} + \hat{n}_j \cos \hat{\Phi}_i} \tag{115}$$

$$\hat{t}_{ijp} = \frac{2 \hat{n}_i \cos \hat{\Phi}_i}{\hat{n}_i \sqrt{1 - (\hat{n}_i/\hat{n}_j)^2 \sin^2 \hat{\Phi}_i} + \hat{n}_j \cos \hat{\Phi}_i} \tag{116}$$

$$\hat{r}_{ijs} = \frac{\hat{n}_i \cos \hat{\Phi}_i - \hat{n}_j \sqrt{1 - (\hat{n}_i/\hat{n}_j)^2 \sin^2 \hat{\Phi}_i}}{\hat{n}_i \cos \hat{\Phi}_i + \hat{n}_j \sqrt{1 - (\hat{n}_i/\hat{n}_j)^2 \sin^2 \hat{\Phi}_i}} \tag{117}$$

and

$$\hat{t}_{01s} = \frac{2 \hat{n}_i \cos \hat{\Phi}_i}{\hat{n}_i \cos \phi_i + \hat{n}_j \sqrt{1 - (\hat{n}_i/\hat{n}_j)^2 \sin^2 \hat{\Phi}_i}} \tag{118}$$

These four relations apply to all TIR and ATR phenomena at the interface of sufficiently thick pieces of optically dense and rare materials, whether or not the media are absorbing.

The inversion of these formulas to obtain the optical constants usually cannot be done exactly, and a computer algorithm such as Marquardt's (Ref. 34) must therefore be used. Approximate solutions for the optical properties of weakly absorbing media are useful and easily obtainable, however, using the concept of effective thickness (Ref. 44). These are found in the next section.

3.1.3 Effective Thicknesses of a Semi-Infinite Weakly Absorbing Rarer Medium

If the semi-infinite incident medium is transparent, and the semi-infinite, or thick ($d >> d_p$), rarer medium is nearly transparent, then to a good approximation, the critical angle, ϕ_{12c}, is that of Eq. (72). The effective penetration depth, d_e, is defined from the relation

$$\left|\hat{r}_{12}\right|^2 \equiv 1 - \alpha d_e \tag{119}$$

where $\alpha = 4\pi k\nu$ is the Lambert absorption coefficient in the Lambert-de Beers law of intensity transmission in the z-direction:

$$dI = -I \alpha \, dz \text{ , or } I = I_o e^{-\alpha z} \tag{120}$$

for intensity, I (Ref. 42).

Harrick (Ref. 47) has considered the low-absorption rarer medium as a perturbation of the nonabsorbing rarer medium situation; he gives for the effective penetration thickness

$$d_e = \frac{n_{21} \left| \hat{T}/\hat{E} \right|^2 d_p}{2 \cos \phi_1}$$

$$= \frac{n_{21} \left| \hat{T}/\hat{E} \right|^2}{4 \pi \nu n_1 \left(\sin^2 \phi_1 - n_{21}^2 \right)^{1/2} \cos \phi_1} \tag{121}$$

where Eq. (105) is substituted. Using either Eq. (111) or Eq. (113) in Eq. (121) produces

$$d_{e_\parallel} = \frac{n_{21} \cos \phi_1 \left(2 \sin^2 \phi_1 - n_{21}^2 \right)^{1/2}}{\pi \nu n_1 \left(1 - n_{21}^2 \right) \left(\sin^2 \phi_1 - n_{21}^2 \right)^{1/2} \left(\sin^2 \phi_1 - n_{21}^2 \cos^2 \phi_1 \right)} \tag{122}$$

or

$$d_{e_\perp} = \frac{n_{21} \cos \phi_1}{\pi \nu n_1 \left(1 - n_{21}^2 \right) \left(\sin^2 \phi_1 - n_{21}^2 \right)^{1/2}} \tag{123}$$

Obviously, an increase in the effective penetration depths can result from decreasing ϕ_1 and/or ν, and better refractive index matching (i.e., letting n_{21} approach 1). Note that $d_{e\parallel}$ is greater than $d_{e_\perp}$ at a given angle of incidence; therefore, the parallel component alone is frequently used in experiments on a thick film.

3.1.4 Effective Thicknessess of a Very Thin Weakly Absorbing Film

In this section, a very thin film is considered to be one whose thickness, d, is very much smaller than the penetration depth computed for two transparent media [Eq. (105)], $d << d_{po}$. Let the very thin film be isotropic, planar, and of complex refractive index, $\hat{n}_2$. The thin film is sandwiched between two semi-infinite transparent media: the incident medium n_1 and the medium n_3.

At the interface of media $\hat{n}_i$ and $\hat{n}_j$, the fraction of the incident power entering the second medium $\hat{n}_j$ is $|\hat{n}_j/\hat{n}_i| \, |\hat{t}_{ij}|^2 \approx (n_j/n_i)|\hat{t}_{ij}|^2$ for transparent or nearly transparent media. If the power is assumed to be constant with film thickness, then Eqs. (111) and (113) must be modified to read (Ref. 42)

$$\left| \frac{\hat{T}_\perp}{\hat{E}_\perp} \right| = \frac{2 \cos \phi_1}{\sqrt{1 - n_{31}^2}} \tag{124}$$

and

$$\frac{\hat{T}_\parallel}{\hat{E}_\parallel} = \frac{2 \cos \phi_1 \left[\left(1 + n_{32}^4 \right) \sin^2 \phi_1 - n_{31}^2 \right]^{1/2}}{\left\{ \left(1 - n_{31}^2 \right) \left(\sin^2 \phi_1 - n_{31}^2 \cos^2 \phi_1 \right) \right\}^{1/2}} \tag{125}$$

where

$$n_{ji} \equiv n_j / n_i \tag{126}$$

For the very thin film, the effective thickness is (Ref. 42)

$$d_e = \frac{n_{21} \left| \hat{T}/\hat{E} \right|^2 d}{\cos \phi_1} \tag{127}$$

which becomes, upon combining with either Eq. (124) or (125), either

$$d_{e_\perp} = \frac{4 d n_{21} \cos \phi_1}{\sqrt{1 - n_{31}^2}} \tag{128}$$

or

$$d_{e_\parallel} = \frac{4 d n_{21} \cos \phi_1 \left[\left(1 + n_{32}^4 \right) \sin^2 \phi_1 - n_{31}^2 \right]^{1/2}}{\left\{ \left(1 - n_{31}^2 \right) \left(\sin^2 \phi_1 - n_{31}^2 \cos^2 \phi_1 \right) \right\}^{1/2}} \tag{129}$$

Here, $d_{e_\parallel}$ may be greater or smaller than $d_{e_\perp}$.

3.2 Experimental Techniques

The two major divisions of internal reflection spectroscopy are single reflection methods, or ATR methods, and multiple internal reflection, or MIR techniques. For both kinds of internal reflection spectroscopy, the proper internal reflection element (IRE) is very important.

3.2.1 Internal Reflection Elements

In Ref. 42, Harrick discusses single and multiple IRE's at length. He notes that the IRE material must have a high, known index of refraction, n, and must be transparent or very nearly so (especially for MIR measurements) because of the possible loss of beam power when the beam is within the IRE.

Although fixed-angle IRE's (such as prisms) are usually simpler to machine, variable-angle IRE's (such as hemicylinders) are necessary if measurements are desired at several angles (Ref. 40). For weakly absorbing samples, the number of multiple absorptions can be increased by designs involving multiple passes of the beam through the IRE.

While there are many IRE materials (such as Ge, KRS-5, and NaCl) whose optical properties are known in the visible and IR regions at 300°K, very few optical constants are known for these or other suitable materials at cryogenic temperatures. Ge has been measured at 20°K and 80°K (Ref. 28), but other cryogenic measurements, especially on KRS-5, should be undertaken.

3.2.2 Single Reflection Methods

If the samples have sufficient absorption, a single reflection technique is often simpler and preferable to the multiple reflection techniques. Many investigators have applied single reflection techniques to studies of thick solids and liquids throughout the IR (Refs. 40, 42, 46, 47, 48, and 49).

In most single reflection studies the incident beam is unpolarized, but the spectrometer optics introduce a partial polarization. If the spectrometer passes a ratio, $S(\nu)$, of perpendicular, s, to parallel, p, intensity at the wavenumber, ν, then the measured quantity, R, is the ratio of the beam intensity, I, when a sample is in contact with the IRE, to the beam intensity, I_o, when no sample is on the IRE. Let $\hat{n}_1$, $\hat{n}_2$, and $\hat{n}_3$ refer, respectively, to the IRE material, the sample, and the ambient. The following results, then, for thick samples

$$I/I_o = R = \left|\hat{r}_{12}\right|^2 \Big/ \left|r_{13}\right|^2 \tag{130}$$

where

$$\left|\hat{r}_{ij}\right|^2 = \frac{\left|\hat{r}_{ijp}\right|^2 + S\left|\hat{r}_{ijs}\right|^2}{1+S} \tag{131}$$

and r_{ijl} is obtained from Eqs. (115) and (116). For a prism instrument, S is nearly constant over a typical absorption band, whereas a grating instrument may have a wildly varying S over the same spectral region (Ref. 46).

For thick samples, Eqs. (115), (116), and (131) show that R is a function of nine parameters: the wavenumber, ν; the angle of incidence; ϕ_1; the instrument polarization function, S; and the real and imaginary parts of $\hat{n}_1$, $\hat{n}_2$, and $\hat{n}_3$. In principle, with at least nine independent measurements of R, one could find the values for all nine parameters at the computed wavenumber. Usually, $k_1 = k_3 = 0$ (i.e., media 1 and 3 are not absorbing), and n_1, n_3, ν, ϕ_1, and S are measured, thereby reducing the number of unknown parameters to the two optical constants, n_1 and k_1, of the thick sample. Inversion of Eq. (130) can only be done iteratively by a computer.

With a single hemicylinder IRE, Crawford et al. (Ref. 46) first measured $S(\nu)$ over the fairly small wavenumber region of interest (typically about 200 cm^{-1}), using a stack of inclined AgCl plates. Using a wide range of incident angles, they then obtained a preliminary determination of the optical constants. They finally used a program which computes an optimum set of angles to be used in the final measurement of the optical constants.

On the other hand, Irons and Thompson (Ref. 49) used several prism IRE's made of different materials; the prisms had different fixed angles of incidence. The optimum angles of incidence were determined empirically for each prism, and several values of R were found at a given wavelength.

3.2.3 Multiple Internal Reflection (MIR) Techniques

MIR techniques are preferable to single reflection methods for spectral regions in which the absorption of thick materials is weak, or for such cases when, the sample for such cases being a very thin film, the absorption of energy per reflection from an incident beam is too small to measure accurately.

If a fraction, R, of the incident intensity is reflected per reflection, then the measured quantity in an MIR experiment with N reflections is the ratio of the beam intensity, I, when a sample is in contact with the IRE, to the beam intensity, I_o, when no sample is on the IRE. Thus,

$$I/I_o = R^N \tag{132}$$

Inversion of Eq. (132) requires a computer algorithm.

In what follows, $\hat{n}_1$ refers to the IRE (dense) material, $\hat{n}_2$ to the sample and $\hat{n}_3$ to the ambient index.

3.2.3.1 MIR Methods for Thick Samples

For samples whose minimum thickness, d, is much larger than the penetration depth, d_p [Eq. (105)], R is the same as given in Eq. (130) for all thick samples. If the radiation is plane-polarized parallel to the plane of incidence (i.e., S = 0), then $R = |r_{12p}|^2/|r_{13p}|^2$, and if polarized perpendicularly (i.e., S = 0), then $R = |\hat{r}_{12p}|^2/|\hat{r}_{13p}|^2$. The measurements I/I_o are functions of 10 parameters: ν, ϕ_1, S, N, and the real and imaginary parts of $\hat{n}_1$, $\hat{n}_2$, and $\hat{n}_3$, of which all but n_2 and k_2 of the sample are usually measured before an MIR experiment.

The use of MIR methods for solid and liquid thick samples is discussed by Rawlins (Ref. 48), Medeck (Ref. 50), and others. (More extensive lists of studies are given in the bibliographies of Refs. 42 and 43.)

3.2.3.2 MIR Methods for Thin Films

If the penetration depth, d_p, is greater or comparable to the film thickness, d, then the proper value for R is

$$R_{film} = \left|\hat{r}_{123}\right|^2 \left|\hat{r}_{13}\right|^2 \tag{133}$$

where

$$\left|\hat{r}_{123}\right|^2 = \frac{\left|\hat{r}_{123p}\right|^2 + \left|\hat{r}_{123s}\right|^2 S}{1+S} \tag{134}$$

and r_{1231} is analogous to r_{0121} in Eq. (67). For polarized radiation, R_{film} is found from the appropriate component values of $\hat{r}_{123}$ and $\hat{r}_{13}$ inserted into Eq. (133). The same 10 parameters appear in Eqs. (130) and (133). As in the thick sample case, though, usually all but the sample optical constants n_1 and k_1 are known. Again, a computer algorithm such as that used by Marquardt (Ref. 34) is required to solve for any unknown parameters.

If the optical constants of thin films are to be determined by MIR, preliminary calculations may be made using the effective depths, given in Section 3.1.4, to find tentative values of the critical angle, an appropriate IRE material, the proper geometry of the IRE, and other experimental parameters. These effective depths may also be used in certain cases to obtain good approximate values of the optical constants of the sample (Ref. 44). The accurate determination of the optical constants may require several experimental runs, however, as well as an analysis of the data using Eq. (133).

Numerous authors have used MIR spectra of thin films for qualitative analyses, rather than for finding the optical properties of the sample. (See Refs. 41, 42, 44, 51, and 52.)

3.3 COMMERCIAL INSTRUMENTATION FOR INTERNAL REFLECTION SPECTROSCOPY (IRS)

Instrumentation for IRS is available from:

1. Barnes Engineering
   Stamford, Connecticut
2. Beckman Instruments, Inc.
   Fullerton, California
3. Perkin-Elmer Corp.
   Norwalk, Connecticut
4. Research and Industrial Instruments Co.
   London, England
5. Foxboro Analytical
   Wilks Infrared Center
   South Norwalk, Connecticut

The pioneering manufacturers were Connecticut Instruments, which built the first commercial IRS attachment for spectrometers in 1965 (and is now a part of Barnes Engineering) and Wilks Scientific Corp. (now a part of the Foxboro Company). The first IRS units were accessories for existing sing- and double-beam spectrometers including single reflection and MIR units. There are now IRS units available for microsamples (with a diamond IRE), for variable-angle MIR spectroscopy, and for skin analyses, and narrow MIR plates made of KRS-5, Ge, Si and ZnSe. There are now specialized IRS spectrometers that can make routine analyses rapidly with microcomputer control.

It is difficult to rate the commercial IRS products available. Most IRS units but not all can be attached to the popular IR spectrometers including Fourier Transform instruments. Some units, however, may be more easily placed in position than others, depending on the spectrometer. As a general rule, the units designed by a manufacturer for its own spectrometers are more easily used with those instruments. The authors have noted that in the articles they have read, Wilks' instrumentation was utilized more than other equipment.

3.4 SUMMARY ON INTERNAL REFLECTION SPECTROSCOPY OF FILMS

In the IR, visible, and near-UV spectral regions, IRS spectra may often be superior to conventional reflection or transmission spectra, especially for weakly absorbing samples or very thin films. IRS techniques may be used in conjunction with ellipsometric measurements on thin films because the IRS measurements are sensitive to the optical constants of the material, and ellipsometer data depend heavily on film thickness. Films having a minimum thickness much greater than the penetration depth of the evanescent field have IRS spectra which are free of multiple reflection effects, even for nonplanar films. Accurate reduction of IRS data for films of any thickness can be done only by computer programs.

Finally, a wide variety of stock items for IRS is currently available for single reflection and MIR studies of liquids and solids.

4.0 ANALYSES OF MOLECULAR ABSORPTION BANDS BY THE METHOD OF MOMENTS

A crucial part of accurate determination of mole fractions of IR-active species in cryodeposits is the calculation of band strengths of those species. Discrepancies noted earlier (Refs. 1 and 2) between calculated mole fractions and those obtained by chemical analysis were thought to be partly caused by experimental uncertainties in the computation of band strengths. In particular, choices of integration limits and background absorption (baseline) were made on an intuitive or empirical rather than quantitative basis. It was recommended at that time that a "moment" method be tried and evaluated in future band strength calculations, as a possible means of reducing experimental uncertainty.

In a series of papers (Refs. 54 through 57), Gordon analyzed vibration bands theoretically in terms of their moments. By using data obtained from various experimental studies, he tested the theoretical analysis for consistency and, in the process, provided a method to determine integration limits and baselines quantitatively. (For related work on band analyses, see Refs. 58 through 66.)

4.1 THE FIRST AND SECOND MOMENTS

Much of the present work was devoted to moment analysis. The scheme adopted follows that suggested by Gordon's work and implemented by Jiang et al. (Ref. 67). The moment method rests on the assumption that the first and second moments of an absorption band are independent of intermolecular forces. Thus, the calculated second moment must match the "classical" second moment plus quantum-mechanical correction terms that become significant at low temperatures.

In general, the nth moment is defined (Ref. 67) by

$$M(n) = \int (\omega - \omega_s)\, p\,(\omega)\, d\omega \Big/ \int p\,(\omega)\, d\omega \tag{135}$$

where ω_s is the "shifted band origin," $p(\omega)$, is an intensity distribution function, and $\omega = 2\pi c\nu$. The shifted origin, ω_s, is chosen so that M(1) agrees with the classical first moment M_1:

$$M(1) = \frac{\int (\omega - \omega_s)\, p\,(\omega)\, d\omega}{\int p\,(\omega)\, d\omega} = M_1 \tag{136}$$

4.2 COMPUTER PROGRAM MOMENT

A moment analysis program has been written using moments converted to ν units with the distribution function $p(\omega) = p(2\pi c\nu) = k(\nu)$. The computer program MOMENT contains five options for $k(\nu)$. AEDC k-values were used in addition to those k-values fitted by nonlinear least squares to the following four models:

$$\begin{aligned} k_c(\nu) &= \frac{a}{1 + c^2 (\nu - b)^2} \\ k_g(\nu) &= f \cdot \exp\left[-d^2 (\nu - b)^2\right] \\ k_p(\nu) &= k_c(\nu) \cdot k_g(\nu) \\ k_s(\nu) &= k_c(\nu) + k_g(\nu) \end{aligned} \tag{137}$$

The models k_c and k_g are the familiar Cauchy (Lorentz) and Gauss profiles; they provide one possible method of treating blended absorption bands (bands such that the band of interest is blended with a lattice vibration). Jones et al. (Refs. 69 through 71) have used nonlinear least squares to fit absorption spectra and, in some instances, have found the product or sum model to give a better fit than the pure Cauchy or Gauss profiles.

Program MOMENT was designed to first calculate the shifted band origin, ν_s, using Eq. (136), and to then force the calculated second moment, M(2), to match the classical second moment, M_2, plus quantum corrections. All calculated moments, M(n), $n \geq 2$ are computed with respect to ν_s, and the equation used is that derived by Gordon (Ref. 58):

$$M(2) = M_2 + \frac{M(4)}{12} \cdot \left(\frac{hc}{kT}\right)^2 - \frac{M(6)}{120} \left(\frac{hc}{kT}\right)^4 + \frac{17\, M(8)}{20{,}100} \left(\frac{hc}{kT}\right)^6 - \ldots \tag{138}$$

The right side of Eq. (138) is an infinite alternating series, convergent whenever $|\nu| < \pi kT/hc \approx 43.67$ and asymptotic outside that interval. An iterative scheme was used in an

attempt to force the quality indicated in Eq. (138), by using corrections through the M(8) term. The (horizontal) baseline height and limits of integration were adjusted (simultaneously, in the case of the model options) for 50 iterations or until agreement of the order 10^{-5} was reached. The limits of integration were chosen to be those ν-values for which the baseline intersected the k-profile. When the AEDC k-values were used, Simpson's rule (modified for unequal subdivisions) was used to calculate the moments; when model options were used, the integrations were performed either analytically or by using 10-point Gaussian quadrature over each of 10 equal subintervals of the integration range.

4.3 ANALYSES WITH PROGRAM MOMENT

The MOMENT program was first used to analyze ν_2 of H_2O, $^{12}CO(1-0)$, and ν_3 of $^{13}CO_2$; AEDC data from 20°K cryofilms were used. The iterative scheme failed to converge in all cases because the calculated second moment, M(2), was so small compared to the classical value, M_2. Either truncation of the wings or insufficient resolution of data in the wings could cause these weak second moments.

All of the models were then fitted by nonlinear least squares to the bands mentioned in the previous paragraph; only one positive result was obtained, that with the Cauchy fit to ν_3 of $^{13}CO_2$. Again, in all but this one case, the calculated second moment was well below the classical value, or, when the baseline and limits were adjusted to achieve a closer agreement between M(2) and M_2, the correction terms became extremely large, and the correction series became divergent. Since accurate representation of absorption bands in the wings is essential for successful moment analysis, the models might require modification or other models might have to be found that better approximate bands in the wings.

Incidentally, the computer results, even in the failed cases, offered empirical evidence of some general results on moment analysis with symmetric models, some of which may be used in practice to determine whether a given model adequately represents $k(\nu)$. Some of these results were verified mathematically and are discussed later in the report.

By using the Cauchy representations of ν_3 of $^{13}CO_2$ in pure CO_2 and in the binary mixture N_2/CO_2, new values were obtained for the band strengths in both the standard cryofilm (pure CO_2) and in the mixture. The moment analysis produced "corrected" baselines and limits of integration which gave excellent agreement between M(2) and the quantum-corrected M_2. The difference $M(2) - M_2$ was less than 10^5 in both cases. The band strength ratio, R, and mole fraction, f, were calculated and compared with previously reported values (Ref. 1). The previous value obtained, $f = 0.296$, is within 17 percent of the mole fraction determined by chemical analysis. The present value obtained, $f = 0.289$ represents a slight improvement, falling within 14.3 percent of the chemically determined value of 0.253.

4.4 MATHEMATICAL BAND MODELS

To help assess the appropriateness of the various mathematical models, it is useful to examine some of their results. It is assumed that each distribution, $k(\nu)$, is symmetric about the band center, b, and that the interval of integration is $(b - \delta, b + \delta)$, $\delta > 0$. (Detailed calculations are given in the Appendix.)

Result 1. The shifted band origin is independent of the baseline and integration limits. In fact, $b - \nu_s = M_1$, the classical first moment.

Result 2. For the Cauchy profile,

$$\lim_{\delta \to \infty} M(n) = \infty \quad \text{for} \quad n \geq 2$$

as Gordon and others have pointed out.

Remark. Curiously, it is this property of $k_c(\nu)$ that makes it possible for our moment analysis to succeed in those cases when $M(2) - M_2$ is sufficiently small and positive.

Result 3. For the Gaussian profile, $k_g(\nu)$, all moments are finite as $\delta \to \infty$. In particular,

$$\lim_{\delta \to \infty} M(2) = \left(1/2d^2\right) + M_1^2 \tag{139}$$

Here $d = 2(\ln 2)^{1/2}/W$, where W is the band width at half height.

Remarks. Equation (139) can be used in practice to decide whether the Gaussian profile is appropriate for a given band. For example, the formula in Eq. (139) yields an upper bound of 5.0052 for M(2), using the ν_3 band of CO_2. (In this analysis, parameters such as d are converged least-squares values for the Gaussian fit to the AEDC data.) The classical second moment for CO_2 is $M_2 = 21.862858$. Thus, the MOMENT analysis method will not succeed for this Gaussian profile, regardless of how the baseline and limits are adjusted, since M(2) has a fixed upper bound far *below* M_2.

Result 4. The higher moments are calculated about the shifted band origin, with baseline $1 = k(b - \delta) = k(b + \delta)$:

$$M(n) = \int (\nu - \nu_s)^n \left[k(\nu) - \ell \right] d\nu \Big/ \int \left[k(\nu) - \ell \right] d\nu \tag{140}$$

These moments can be rewritten in terms of moments about the axis of symmetry, $\nu = b$, where b is the band center. The *even* moments, in particular, are given as:

$$M(2n) = \left[\sum_{j=0}^{n} \binom{2n}{2j} M_1^{2j} \cdot M_b (2n - 2j) - T \right] \Big/ (J - 2\ell\delta)$$

where

$$T = (\ell/2n + 1) \left[(\delta + M_1)^{2n+1} + (\delta - M_1)^{2n+1} \right]$$

$$M_b(n) = \int (\nu - b)^n \, k(\nu) \, d\nu$$

and

$$J = \int k(\nu) \, d\nu = M_b(0)$$

Remark. Writing the moments in this manner allows the integration to be done analytically for the models in Eq. (137). We rewrote the moment program for the Cauchy model on a Radio Shack® TRS-80 microcomputer, doing all integrations analytically, and obtained results very similar to those of the original MOMENT program. The rewritten program should and, we believe, did give slightly better values for the moments and band integrals.

4.5 COMPARISON WITH OTHER MOMENT ANALYSES

All of the above analysis dealt with 20°K cryofilms. In addition to these attempts, we tried to duplicate the results of Jiang et al. (Ref. 69) using their band parameters and a Cauchy model for the band $^{12}CO(1 \leftarrow 0)$ at 30°K. This attempt failed, again because of a very weak calculated second moment compared to the classical value. Thus, it may be instructive to consider some of the differences between the present analysis and that of Jiang et al. First, they used the distribution function $p(\omega) = \ell n(Io/I)$ from an absorbance measurement, while the present research involved $k(\nu)$ fitted by a Cauchy model.

Jiang et al. integrated geometrically (band integrals, for example, were calculated either from data plots or directly from the spectrum using a polar planimeter), getting best results for a baseline that matched the intensity in the wings and followed "the estimated fringe pattern for a hypothetical thin nonabsorbing CO film." The model used in the present study for $k(\nu)$ is smooth in the wings, with "channel spectra" eliminated. Also, horizontal baselines were tried and symmetric limits chosen. The only limits given by Jiang, et al. were in a footnote; they were those limits applied to an Ar/CO mixture at 30°K. These limits were not quite symmetric about the band origin, thus giving a slightly different shifted band origin from the present results. Incidentally, better results were achieved in the present study by choosing skewed limits.

4.6 SUMMARY ON MOMENTS

The present modest success with moment analysis proves that the technique deserves further examination and refinement and that the questions implied by the above discussion warrant investigation. In particular, questions remain to be answered concerning which models are best to use for the intensity distribution function and how the limits of integration should be determined as the baseline is adjusted.

The independence of the second moment, M(2), from intermolecular interactions (Refs. 55, 56, and 57) especially warrants scrutiny. It is hoped that a method can be developed centering in this characteristic that would allow spectroscopic determinations of species concentration in a cryofilm regardless of which species are in the film.

5.0 SUMMARY

We have investigated the applicability of the ellipsometric and internal reflection spectroscopy (IRS) methods of reflection spectroscopy to measurements of the optical properties of thin films and substrates. Ellipsometry is very sensitive to the condition of sample surfaces and film structure and can accurately measure optical constants of films and their thicknesses, even in the case of multiple films. The technique can be used to make optical measurements of substrates, but these data must be treated with reserve because of the possibility of spurious effects caused by molecular absorption. Ellipsometric measurements in the IR beyond 3 μm require special methods and instrumentation and are not as accurate as observations in the visible range.

On the contrary, IRS data can easily be obtained throughout the IR spectral range as well as the visible. The penetration of the evanescent wave makes IRS more a probe of the bulk properties of thick samples rather than of their surface characteristics. By prudent choices of the beam incident angle and, thus, of the penetration depth, one may obtain spectra of strong *or* weak absorption features that have higher resolution than do transmission spectra or other reflection data. Accurate IRS data of thinner films are also made possible if multiple reflection effects with the film are accounted for. One may also capitalize on the lower power loss per reflection and use multiple internal reflection (MIR) schemes for weakly absorbing (thick or thin) samples.

To extract accurate optical constants and film thicknesses from either of the above reflectance methods, researchers must perform a computer inversion of the appropriate equations. Because of the numerous methods of ellipsometric or IRS measurements, local algorithms are necessary for handling the experimental configuration.

The analysis of molecular absorption band moments can lead to a quantitative evaluation of the intermolecular interactions of molecules in condensed phases. These interactions cause spectral distortions that make molecular species concentration determinations difficult. A preliminary investigation of moment analysis shows that symmetric band shapes must meet some simple criteria in order to find an accurate value of the band strength. Also, the importance of accurate profiles of the wings of an absorption band in moment analysis must be emphasized. It is, perhaps, because of this fact that higher-resolution data are necessary for meaningful moment analysis. It is also hoped that the lack of dependence of the second moment upon the intermolecular interactions can lead to a way of finding molecular concentrations in mixtures varying widely in their constituents.

Other areas of consideration for future research are:

1. analysis of the physics of quartz crystal microbalances (QCM),

2. computer programming for the analysis of ellipsometric and IRS data,

3. investigation of the effect of multiple reflections in a dielectric substrate during ellipsometric measurements,

4. continuation of moment analysis and the determination of molecular species concentrations in cryofilms,

5. completion of the computer program (now in its final debugging stage) for Kramers-Kronig (KK) analysis of the transmission of a beam through a single thickness thin film, and

6. completion of the computer program for KK analysis of the reflection of a beam of a single thickness of a thin film.

REFERENCES

1. Palmer, K. F. "Methods to Quantify Constituents in Binary Cryodeposits." Participant's Final Report, 1976 USAF-ASEE Summer Faculty Research Program, AEDC.

2. Palmer, K. F., Roux, J. A., and Wood, B. E. "Analysis of Cryodeposit Mixtures." AEDC-TR-79-80 (AD-A084548), May 1980.

3. Neal, W. E. J. "Application of Ellipsometry to Surface Film and Film Growth." *Surface Technology*, Vol. 6, 1977, pp. 81-110.

4. Azzam, R. M. A. and Bashara, N. M. *Ellipsometry and Polarized Light*. North-Holland Publishing Co., Amsterdam, The Netherlands, 1977.

5. Ditchburn, R. W. *Light*. Third edition, Vols. 1 and 2. Academic Press, New York, 1976.

6. Spanier, R. F. "Ellipsometry: A Century-Old New Technique." *Industrial Research*, September 1975, pp. 73-76.

7. Muller, R. H. "Definitions and Conventions in Ellipsometry." *Surface Science*, Vol. 16, 1969, pp. 14-33.

8. Roberts, R. H. "On Determining Optical Constants of Metals in the Infrared." In *Ellipsometry in the Measurement of Surfaces and Thin Films*, eds. Passaglia, E., Stromberg, R. R., and Kruger, J. U.S. Government Printing Office, Washington, D.C., 1964, pp. 119-127.

9. Winterbottom, A. B. "Increased Scope of Ellipsometric Studies of Surface Film Formation." In *Ellipsometry in the Measurement of Surfaces and Thin Films*. U.S. Government Printing Office, Washington, D.C., 1964, pp. 97-112.

10. Bennett, H. E. and Bennet, J. M. "Precision Measurements in Thin Film Optics." In *Physics of Thin Films*, Vol. 4, eds. Hass, G. and Thun, R. E. Academic Press, New York, 1967.

11. Partington, J. R. *An Advanced Treatise on Physical Chemistry*, Vol. 4. Longman, Greens and Co., London, 1953.

12. Plumb, R. C. "Analysis of Elliptically Polarized Light." *Journal of the Optical Society of America*, Vol. 52, 1962, p. 1410.

13. Archer, R. J. *Ellipsometry*. Gaertner Scientific Corp., Chicago, Illinois, 1968.

14. Archer, R. J. and Shank, C. V. "Ellipsometry with Non-Ideal Compensators." *Journal of the Optical Society of America*, Vol. 57, No. 2, February 1967, pp. 191-194.

15. O'Bryan, H. M. "The Optical Constants of Several Metals in Vacuum. *Journal of the Optical Society of America*, Vol. 26, No. 3, March 1936, pp. 122-127.

16. Zaghloul, A.-R. M. "Modified O'Bryan Ellipsometer (MOE) for Film-Substrate Systems." *Optics Communications*, Vol. 27, No. 10, October 1978, pp. 1-3.

17. Kinsoita, K. and Yamamoto, M. "Principal Angle-of-incidence Ellipsometry." *Surface Science*, Vol. 56, 1976, pp. 64-75.

18. So, S. S. and Vedam, K. "Generalized Ellipsometric Method for the Absorbing Substrate Covered with a Transparent-Film System. Optical Constants of Silicon at 3655 Å." *Journal of the Optical Society of America*, Vol. 62, No. 1, January 1972, pp. 16-23.

19. Vergnez, F. and Dupont-Pavlovsky, N. "Ellipsometry without a Compensator—Two Improvements in Speed and Reliability of the Monin and Boutry Method." *Optics Communications*, Vol. 32, No. 1, January 1980, pp. 5-10.

20. Stobie, R. W., Rao, B., and Dignam, M. J. "Analysis of a Novel Ellipsometric Technique with Special Advantages for Infrared Spectroscopy." *Journal of the Optical Society of America*, Vol. 65, No. 1, January 1975, pp. 25-28.

21. Dignam, M. J., Rao, B., and Stone, R. W. "IR Ellipsometric Spectroscopy: Its Application to Butanol Absorbed on Silver." *Surface Science*, Vol. 46, 1974, pp. 308-310.

22. De Smet, D. J. "Ellipsometry of Anisotropic Surfaces." *Journal of the Optical Society of America*, Vol. 63, No. 8, August 1973, pp. 958-964.

23. Heavens, O. S. *Optical Properties of Thin Films*. Dover Publications, Inc., New York, 1965.

24. Ditchburn, R. W. "Some New Formulas for Determining the Optical Constants from Measurements on Reflected Light." *Journal of the Optical Society of America*, Vol. 45, No. 9, September 1955, pp. 743-748.

25. Born, M. and Wolf, E. *Principles of Optics*. Fifth Edition. Pergamon Press, Oxford, 1975.

26. Vasicek, A. "Optical Study of a Thin Absorbing Film on a Metal Surface." In *Ellipsometry in the Measurement of Surfaces on Thin Films*. U.S. Government Printing Office, Washington, D.C., 1964, pp. 25-39.

27. For example: Arnold, F., Sanderson, R. B., Mantz, A. W. and Thompson, S. B. "Infrared Spectral Reflectance of Plume Species on Cooled Low Scatter Mirrors." AFRPL-TR-73-52, September 1973.

28. For example: Ref. 2, and Pipes, J. G., Roux, J. A., Smith, A. M., and Scott, H. E. "Infrared Transmission of Contaminated Cryocooled Optical Windows. *AIAA Journal*, Vol. 16, No. 9, September 1978, pp. 984-990.

29. Burge, D. K. And Bennett, H. E. "Effect of a Thin Surface Film on the Ellipsometric Determination of Optical Constants." *Journal of the Optical Society of America*, Vol. 54, No. 12, December 1964, pp. 1428-1433.

30. McCrackin, F. L. "A Fortran Program for Analysis of Ellipsometer Measurements." NBS TN-479, April 1969.

31. Idczac, E., Oleszkiewicz, E., and Zukowska, K. "An Algorithm for Determining the Refractive Index and Thickness of Thin Dielectric Layers on an Absorbing Substrate on the Basis of Ellipsometric Measurements." *Optica Applicata*, Vol. 9, 1979, pp. 47-50.

32. McCrackin, F. L. and Colson, J. P. "Computational Techniques for the Use of the Exact Drude Equations in Reflection Problems." In *Ellipsometry in the Measurement of Surfaces and Thin Films*. Government Printing Office, Washington, D.C., 1964, pp. 61-82.

33. For example: See the references cited in Refs. 3 and 4.

34. Marquardt, D. W. "An Algorithm for Least-Squares Estimation of Nonlinear Parameters." *Journal of the Society for Industrial and Applied Mathematics*, Vol. 11, No. 2, June 1963, pp. 431-441.

35. Tempelmeyer, K. E. and Mills, D. W., Jr. "Refractive Index of Carbon Dioxide Cryodeposit." *Applied Optics*, Vol. 16, 1968, pp. 2968-2969.

36. Popov, W. A. "Ellipsometry: Zeroing in on Thin Films." *Optical Spectra*, Vol. 11, No. 5, May 1977, pp. 25-27.

37. *Bulletin EH*. Gaertner Scientific Co., Chicago, Illinois.

38. *Bulletin 540*. Rudolph Research, Fairfield, N. J.

39. Young, T. R. and Fath, J. M. "Ellipsometry for Frustrated Total Reflection." In *Ellipsometry in the Measurement of Surfaces and Thin Films*. Government Printing Office, Washington, D.C., 1964, pp. 115-125.

40. Fahrenfort, J. "Attenuated Total Reflection: A New Principle for the Production of Useful Infra-red Reflection Spectra of Organic Compounds." *Spectrochimica Acta*, Vol. 17, 1961, pp. 698-707. Fahrenfort, J. and Viszer, V. M. "On the Determination of Optical Constants in the Infrared by Attenuated Total Reflection." *Spectrochimica Acta*, Vol. 18, 1962, pp. 1103-1116.

41. Harrick, N. J. "Total Internal Reflection and its Application to Surface Studies." *Annals of the New York Academy of Sciences*. Vol. 101, January 1963, pp. 928-959.

42. Harrick, N. J. *Internal Reflection Spectroscopy*. Interscience Publishers, New York, 1967.

43. Wilks, P. A., Jr. and Hirschfeld, T. "Internal Reflection Spectroscopy." *Applied Spectroscopy Reviews*, Vol. 1, No. 1, 1967, pp. 99-130.

44. Harrick, N. J. "Electric Field Strengths at Totally Reflecting Interfaces." *Journal of the Optical Society of America*, Vol. 55, No. 7, July 1965, pp. 851-857.

45. Harrick, N. J. and duPre', F. K. "Effective Thickness of Bulk Materials and of Thin Films for Internal Reflection Spectroscopy." *Applied Optics*, Vol. 5, No. 11, November 1966, pp. 1739-1743.

46. Gilby, A. C., Burr, J., Jr., and Crawford, B., Jr. "Vibrational Intensities. XII. An Optical-Mechanical System from Infrared Attenuated Total Reflection Measurements." *Journal of Physical Chemistry*, Vol. 70, No. 5, May 1966, pp. 1520-1524. Gilby, A. C., Burr, J., Jr., Krueger, W., and Crawford, B., Jr. "XIII. Reduction of Attenuated Total Reflection Data to Optical Constants." *J. Phys. Chem.*, Vol. 70, No. 5, May 1966, pp. 1525-1535. Clifford, A. A. and Crawford, B., Jr." XIV. The Relation of Optical Constants to Molecular Parameters." *J. Phys. Chem*, Vol. 70, No. 5, May 1966, pp. 1536-1543.

47. Katlafsky, B. and Keller, R. E. "Attenuated Total Reflectance Infrared Analysis of Aqueous Solutions." *Analytical Chemistry*, Vol. 35, No. 11, October 1963, pp. 1665-1670.

48. Rawlins, T. G. R. "Attenuated Total Reflection Spectroscopy." *Canadian Spectroscopy*, October 1963, pp. 12-16.

49. Irons, G. M. and Thompson, H. W. "Determination of Optical Constants and Vibrational Band Intensities of Liquids in the Infrared Using Attenuated Total Reflexion." Royal Society of London *Proceedings, Series A*, Vol. 298, 1966, pp. 160-177.

50. Medeck, E. "Some Qualitative and Quantitative Applications of Multiple Internal Reflection Spectroscopy." *Canadian Spectroscopy*, May 1968, pp. 76-80.

51. Wilks, P. A., Jr. "Internal Reflectance Spectroscopy I: Effect of Angle of Incidence Change." *Applied Spectroscopy*, Vol. 22, No. 6, November/December 1968, pp. 782-784.

52. Wilks, P. A., Jr. "Internal Reflectance Spectroscopy II: Quantitative Analysis Aspects." *Applied Spectroscopy*, Vol. 23, No. 1, January/February 1969, pp. 63-66.

53. Burdick, D. L. "Absorption Coefficient of NaF by Attenuated Total Reflection Spectroscopy." In *Laser-Induced Damage in Optical Materials*: 1978, eds. Glass, A. J. and Guenther, A. H. National Bureau of Standards Special Publication, Boulder, Colorado, 1978, pp. 13-18.

54. Gordon, R. G. "Three Sum Rules for Total Optical Absorption Cross Sections." *Journal of Chemical Physics*, Vol. 38, No. 7, April 1963, pp. 1724-1729.

55. Gordon, R. G. "Molecular Motion and the Moment Analysis of Molecular Spectra in Condensed Phases. I. Dipole-Allowed Spectra." *Journal of Chemical Physics*, Vol. 39, No. 11, December 1963, pp. 2788-2797.

56. Gordon, R. G. "Molecular Motion and the Moment Analysis of Molecular Spectra. II. The Rotational Raman Effect." *Journal of Chemical Physics*, Vol. 40, No. 7, April 1964, pp. 1973-1985.

57. Gordon, R. G. "Molecular Motion and the Moment Analysis of Molecular Spectra. III. Infrared Spectra." *Journal of Chemical Physics*, Vol. 41, No. 6, September 1964, pp. 1819-1829.

58. Ewing, G. E. and Pimentel, G. C. "Infrared Spectrum of Solid Carbon Monoxide." *Journal of Chemical Physics*, Vol. 35, No. 3, September 1961, pp. 925-930.

59. Ewing, G. E. "Infrared Spectra of Liquid and Solid Carbon Monoxide." *Journal of Chemical Physics*, Vol. 37, No. 10, 15 November 1962, pp. 2250-2256.

60. Berne, B. J., Jortner, J., and Gordon, R. "Vibrational Relaxation of Diatomic Molecules in Gases and Liquids." *Journal of Chemical Physics*, Vol. 47, No. 5, September 1967, pp. 1600-1608.

61. Shimizu, H. "Time-Correlation Function of Molecular Random Motion and Shape of Spectral Bands." *Journal of Chemical Physics*, Vol. 43, No. 7, October 1965, pp. 2453-2465.

62. Shimizu, H. "Dependence of the Time-Correlation Functions of Molecular Random Motions on the Intermolecular Potential." *Journal of Chemical Physics*, Vol. 48, No. 6, March 1968, pp. 2494-2501.

63. Bratož, S., Rias, J., and Guissani, Y. "Infrared Study of Liquids. I. The theory of the IR Spectra of Diatomic Molecules in Inert Solutions." *Journal of Chemical Physics*, Vol. 52, No. 1, January 1970, pp. 439-453.

64. Gordon, R. G. "Relations between Raman Spectroscopy and Nuclear Spin Relaxation." *Journal of Chemical Physics*, Vol. 42, No. 10, May 1965, pp. 3658-3665.

65. Gordon, R. G. "Molecular Motion in Infrared and Raman Spectra." *Journal of Chemical Physics*, Vol. 43, No. 4, August 1965, pp. 1307-1312.

66. Gordon, R. G. "Lattice Combination Bands in Infrared Spectra of Molecular Solids." *Journal of Chemical Physics*, Vol. 37, No. 11, December 1962, pp. 2587-2594.

67. Jiang, G. J., Person, W. B., and Brown, K. G. "Absolute Infrared Intensities and Band Shapes in Pure Solid CO and CO in Some Solid Matrices." *Journal of Chemical Physics*, Vol. 62, No. 4, February 1975, pp. 1201-1211.

68. Jones, R. N., Seshadri, K. S., Jonathan, N. B. W., and Hopkins, J. W. "A Statistical Approach to the Analysis of Infrared Band Profiles." *Canadian Journal of Chemistry*, Vol. 41, No. 3, March 1963, pp. 750-762.

69. Jones, R. N. "The Measurement of Infrared Spectra with Digitally Recording Spectrophotometers." *Pure and Applied Chemistry*, Vol. 18, 1969, pp. 303-321.

70. Jones, R. N. "Computer Programs for Absorption Spectrophotometry." *Applied Optics*, Vol. 8, No. 3, March 1969, pp. 597-601.

71. Young, R. P. and Jones, R. N. "The Shapes of Infrared Absorption Bands of Liquids." *Chemical Reviews*, Vol. 71, No. 2, April 1971, pp. 210-228.

APPENDIX

Here are established the report's results concerning moment analysis with symmetric models.

Result 1. The shifted band origin, ν_s, is calculated as follows:

$$\int (\nu - \nu_s)\, k(\nu)\, d\nu \Big/ \int k(\nu)\, d\nu = M_1$$

Thus,

$$M_1 = \left[\int (\nu - b)\, k(\nu)\, d\nu + \int (b - \nu_s)\, k(\nu)\, d\nu \right] \Big/ \int k(\nu)\, d\nu$$

$$= b - \nu_s$$

since $\int (\nu - b)\, k(\nu)\, d\nu = 0$. This follows from the facts that $k(\nu)$ is symmetric about $\nu = b$ and that the integration interval is $(b - \delta, b + \delta)$ for $\delta > 0$. The same result follows if $k(\nu)$ is replaced by $k(\nu) - 1$, since this latter distribution has the same symmetry properties as $k(\nu)$, and the new limits of integration will remain symmetric about b.

Result 2. It is easy to see that the moments M(n), $n \geq 2$, for the Cauchy model become infinite as the interval of integration becomes infinite. In general, for any symmetric model $k(\nu)$,

$$M(n) = \int (\nu - \nu_s)^n \left[k(\nu) - \ell \right] d\nu \Big/ \int \left[k(\nu) - \ell \right] d\nu$$

If $J = \int k(\nu) d\nu$, then

$$M(n) = \frac{\left\{ \int \left[(\nu - b) + (b - \nu_s) \right]^n k(\nu)\, d\nu - \left[\frac{\ell}{n+1} (\nu - \nu_s)^{n+1} \right]_{b-\delta}^{b+\delta} \right\}}{J - 2\ell\delta}$$

Binomial expansion in the first term of the numerator yields

$$M(n) = \left[\int \sum_{j=0}^{n} \binom{n}{j} (\nu - b)^{n-j} (b - \nu_s)^j\, k(\nu)\, d\nu - T \right] \Big/ (J - 2\ell\delta)$$

where

$$T = \left[\left(\frac{\ell}{n+1} \right) (\nu - \nu_s)^{n+1} \right]_{b-\delta}^{b+\delta} = \left(\frac{\ell}{n+1} \right) \left[(\delta - M_1)^{n+1} + (\delta - M_1)^{n+1} \right]$$

Because of symmetry, the odd moments about b are zero, so

$$M(n) = \left[\sum_{j=0}^{p} \binom{n}{2j} M_1^{2j} M_b(n-2j) - T \right] \Big/ (J - 2\ell\delta) \tag{141}$$

where p is the greatest integer in n/2 and

$$M_b(n) = \int (\nu - b)^n k(\nu)\, d\nu, \qquad M_1 = b - \nu_s$$

For the Cauchy model,

$$M_b(j) = a \int (\nu - b)^j \Big/ \left[1 - c^2 (\nu - b)^2 \right] d\nu$$

$$= \frac{a}{c^{j+1}} \int_{-c\delta}^{c\delta} \frac{u^j}{1 + u^2}\, du$$

For $j \geq 2$, and even,

$$M_b(j) = \frac{2a}{c^{j+1}} \int_0^{c\delta} \frac{u^j}{1 + u^2}\, du$$

and is divergent as $\delta \to \infty$.

Result 3. We derive Eq. (139). From the general calculation above in Result 2,

$$M(2) = \left\{ M_b(2) - M_1^2 J - (\ell/3) \left[(M_1 + \delta)^3 + (M_1 - \delta)^3 \right] \right\} \Big/ (J - 2\ell\delta)$$

Now,

$$(M_1 - \delta)^3 + (M_1 - \delta)^3 = 2\delta (3M_1^2 + \delta^2)$$

Therefore,

$$M(2) = \left[M_b(2) + M_1^2 J - (2\delta\ell/3) \left(3M_1^2 + \delta^2 \right) \right] \Big/ (J - 2\ell\delta)$$

$$= \frac{M_b(2) - 2\ell\delta^3/3}{J - 2\ell\delta} + M_1^2$$

For the Gaussian model,

$$M_b(2) = \int_{b-\delta}^{b+\delta} (\nu - b)^2 \cdot f \cdot e^{-d^2 (\nu - b)^2}\, d\nu$$

If $u = d(\nu - b)$, then

$$M_b(2) = \int_{-d\delta}^{d\delta} \left(u^2/d^2\right) \cdot f \cdot e^{-u^2}\, du/d$$

$$= \left(f/d^3\right) \cdot \int_{-d\delta}^{d\delta} u^2 e^{-u^2}\, du = \left(\frac{2f}{d^3}\right) \int_0^{d\delta} u^2 e^{-u^2}\, du$$

$$= f/d^3 \left(-d\delta e^{-d^2\delta^2} + \int_0^{d\delta} e^{-u^2}\, du \right)$$

$$= -\frac{f\delta}{d^2} e^{-d^2\delta^2} + \frac{J}{2d^2}$$

Thus,

$$M(2) = \frac{J/2d^2 - (f\delta/d^2)\, e^{-d^2\delta^2} - 2\ell\delta^3/3}{J - 2\ell\delta} + M_1^2$$

$$= \frac{J - 2f\delta e^{-d^2\delta^2} - (4/3)\ell d^2\delta^3}{2d^2\,(J - 2\ell\delta)} + M_1^2$$

Now, $fe^{-d^2\delta^2} = \ell$, so $\ell \to 0$ exponentially as $\delta \to \infty$, and

$$\lim_{\delta \to \infty} M(2) = \frac{1}{2d^2} + M_1^2$$

Result 4. This result is established above in deriving Result 2. From Eq. (141), we need only replace n with 2n.